Renal -intercalated cells maintain body fluid and electrolyte balance

Gueutin, Victor ; Vallet, Marion ; Jayat, Maximilien ; Peti-Peterdi, Janos ; Cornière, Nicolas ; Leviel, Françoise ; Sohet, Fabien ; Wagner, Carsten A ; Eladari, Dominique ; Chambrey, Régine

Abstract: Inactivation of the B1 proton pump subunit (ATP6V1B1) in intercalated cells (ICs) leads to type I distal renal tubular acidosis (dRTA), a disease associated with salt- and potassium-losing nephropathy. Here we show that mice deficient in ATP6V1B1 (Atp6v1b1-/- mice) displayed renal loss of NaCl, K+, and water, causing hypovolemia, hypokalemia, and polyuria. We demonstrated that NaCl loss originated from the cortical collecting duct, where activity of both the epithelial sodium channel (ENaC) and the pendrin/Na+-driven chloride/bicarbonate exchanger (pendrin/NDCBE) transport system was impaired. ENaC was appropriately increased in the medullary collecting duct, suggesting a localized inhibition in the cortex. We detected high urinary prostaglandin E2 (PGE2) and ATP levels in Atp6v1b1-/- mice. Inhibition of PGE2 synthesis in vivo restored ENaC protein levels specifically in the cortex. It also normalized protein levels of the large conductance calcium-activated potassium channel and the water channel aquaporin 2, and improved polyuria and hypokalemia in mutant mice. Furthermore, pharmacological inactivation of the proton pump in -ICs induced release of PGE2 through activation of calcium-coupled purinergic receptors. In the present study, we identified ATP-triggered PGE2 paracrine signaling originating from -ICs as a mechanism in the development of the hydroelectrolytic imbalance associated with dRTA. Our data indicate that in addition to principal cells, ICs are also critical in maintaining sodium balance and, hence, normal vascular volume and blood pressure.

DOI: https://doi.org/10.1172/JCI63492

Pivotal role of β-intercalated cells in maintaining body fluid and electrolyte balance

Victor Gueutin[1#], Marion Vallet[2,3], Maximilien Jayat[4], Janos Peti-Peterdi[5], Nicolas Cornière[2,3], Françoise Leviel[1,2,3], Fabien Sohet[1], Carsten A. Wagner[6], Dominique Eladari[2,3,4], and Régine Chambrey[4]

[1]INSERM UMRS 872, Centre de Recherche des Cordeliers, 15 rue de l'Ecole de Médecine, F-75006, Paris, France

[2]Faculté de Médecine Paris-Descartes, 15 rue de l'Ecole de Médecine, F-75006, Paris, France

[3]Hopital Européen Georges Pompidou, Département de Physiologie, Assistance Publique-Hopitaux de Paris, 20 rue Leblanc, F-75015, Paris France

[4]INSERM U970, Paris Cardiovascular Research Center; Université Paris-Descartes , 56 rue Leblanc, F-75015 Paris, France

[5]Department of Physiology and Biophysics, Keck School of Medicine, Zilkha Neurogenetic Institute, University of Southern California, Los Angeles, California 90033, USA

[6]Institute of Physiology and Zurich Center for Integrative Human Physiology (ZIHP), University of Zurich, CH-8057 Zurich, Switzerland

Corresponding author:
Régine Chambrey
INSERM UMR 970, PARCC, 56 rue Leblanc, F-75015, Paris, France
Phone: +33 1 53 98 81 17
Fax +33 1 53 98 79 52
E-mail: regine.chambrey@inserm.fr

[#] **Gueutin V, Vallet M and Jayat M have equally contributed to this work**

The authors have declared that no conflict of interest exists

ABSTRACT

Inactivating mutations of the B1 proton pump subunit (ATP6V1B1) expressed in intercalated cells (ICs) lead to type I distal renal tubular acidosis (dRTA), a disease often associated with a salt and potassium losing nephropathy. Here we show that mice with disruption of the B1 proton pump subunit gene, despite the absence of overt acidemia, display a renal loss of NaCl, K^+ and water causing hypovolemia, hypokalemia and polyuria. We demonstrate that NaCl loss originates from the cortical collecting duct (CD) where activities of both ENaC in principals cells (PCs) and pendrin in β-ICs were impaired. In contrast, ENaC was appropriately up-regulated in medullary CD, suggesting that a local factor inhibits ENaC in the cortex. Accordingly, we detected high urinary PGE_2 and ATP levels in mutant mice, and blockade of PGE_2 synthesis in vivo by indomethacin normalized ENaC protein levels in the cortex but not in the medulla. Indomethacin also improved polyuria and hypokalemia and restored normal AQP2 and BKCa protein levels in mutant mice. Further, pharmacological inactivation of the proton pump in β-ICs induced release of PGE_2 through activation of calcium-coupled purinergic receptors. In the present study, we identify ATP-triggered PGE_2 paracrine signaling originating from β-ICs as a pivotal mechanism in the development of hydro-electrolytic imbalance associated with dRTA. These studies also challenge the existing paradigm on the exclusive role of PCs and offer the new view that ICs and PCs are both critical in maintaining sodium balance, and hence, normal vascular volume and blood pressure.

INTRODUCTION

The distal parts of the nephron, *i.e.* the connecting tubule and the collecting duct, play a critical role in renal acid excretion, and hence, in acid-base homeostasis (1, 2). Acid secretion is achieved by α-intercalated cells (α-ICs), a highly specialized renal cell type expressing an apical vacuolar H^+-ATPase (v-H^+-ATPase) and a basolateral Cl^-/HCO_3^- exchanger kAE1 (3, 4). Protons generated from the hydration of CO_2 within these cells are extruded actively across the apical membrane by the pump, while bicarbonate ions, which are also produced by this process, are translocated across the basolateral membrane by AE1. Dysfunction of either the pump or the anion exchanger can block proton secretion (1, 2). This failure of α-IC to decrease urine pH results in insufficient acid excretion and accumulation of acid in the body. This defect characterizes "classical" (or type 1) distal renal tubular acidosis (dRTA). Accordingly, inactivating mutations of *ATP6V1B1* (5) or *ATP6V0A4* (6) genes, which encode the B1 or the a4 subunits of the proton pump, respectively, or mutations of *SLC4A1* (7, 8), the gene encoding for the Cl^-/HCO_3^- exchanger kAE1 have been identified in patients with the inherited form of type I dRTA (4).

The characteristics of dRTA are not limited to abnormal acid-base balance, *i.e.* to acidemia of variable intensity, but often include a salt- and potassium-losing nephropathy that may lead to renal hypokalemia and dehydration (9, 10). dRTA is also almost invariably complicated by a marked hypercalciuria resulting in kidney stones, bone demineralization, nephrocalcinosis, and ultimately chronic renal failure. Since α-ICs are dedicated to acid secretion and are not thought to play a role in sodium absorption or in potassium secretion, the pathophysiology of the aforementioned sodium and potassium losses observed in patients suffering from dRTA is not well understood. These losses were initially believed to be consecutive to a direct effect of acidosis to depress several transporters along the nephron (11). However, Sebastian et al. demonstrated that sustained correction of acidemia in patients suffering from type I dRTA does not reverse the abnormalities in renal sodium or potassium handling (9, 10). Based on these observations, the authors concluded that impairments in renal sodium and potassium conservation may not be a reversible consequence of acidosis but instead may be consecutive to chronic interstitial nephropathy and nephrocalcinosis. However, the molecular defects that lead to inactivation of the proton pump, i.e., inactivating mutations of *ATP6V1B1* or *ATP6V0A4*, which are frequent mutations observed in human patients, are not expected to affect only α-ICs. In fact, the proteins encoded by these genes are

also expressed by the β (or base-secreting) subtype of IC (β-ICs) that is also present in the distal nephron (12, 13). These cells share some of the characteristics with the α-ICs but with an opposite polarity, i.e., they express the v-H^+-ATPase basolaterally and the Cl^-/HCO_3^- exchanger pendrin (SLC26A4) at their apical membrane (14). Until recently, β-ICs were thought to be exclusively involved in base secretion. However, this paradigm has been challenged by recent observations showing that β-ICs exhibit electroneutral NaCl absorption (15, 16) and participate in the renal regulation of extracellular volume and blood pressure (17, 18). In β-ICs, apical Cl^- influx, which occurs through the Cl^-/HCO_3^- exchanger Pendrin, is linked to apical Na^+ influx by the Na^+-driven Cl^-/HCO_3^- exchanger NDCBE (15, 16). Thus, in theory, mutations that affect directly the proton pump are expected to impair both α-IC and β-IC functions, and thereby affecting not only acid secretion but also NaCl absorption.

Finberg et al. generated a mouse model with disruption of the *Atp6v1b1* gene encoding for the β1 subunit of the H^+-ATPase as a model of human dRTA. As expected from human studies, mice with *Atp6v1b1* disruption (*Atp6v1b1*$^{-/-}$) exhibit an impaired response to acid-loading (19). However, these mice slightly differ from patients in that they do not have overt acidemia under standard laboratory conditions. They also do not exhibit hypercalciuria, and they develop neither nephrocalcinosis, nor interstitial nephritis. Hence, these knockout mice represent an interesting model to study the mechanisms that account for impaired sodium and potassium conservation in patients with dRTA consecutive to dysfunction of the proton pump, and particularly, to assess the involvement of β-IC dysfunction in this model.

Therefore, our goal was to determine whether *Atp6v1b1* disruption leads to a salt- and potassium-losing nephropathy as observed in human dRTA, and then to determine the mechanisms by which dysfunction of the proton pump affects the transport of Na^+, Cl^- and K^+. Here we report that impaired renal sodium and potassium conservation observed in type I dRTA is not the consequence of acidosis or of chronic interstitial nephritis, but is instead the consequence of the proton pump defect in β-ICs. We demonstrate that in mice with *Atp6v1b1* disruption β-ICs impair functions of neighboring principal cells, which normally transport sodium, water and potassium, through paracrine ATP/PGE_2 signaling cascade. Furthermore, gain of ATP-triggered PGE_2 signaling alters electrolytes and water balance in a paracrine manner. Beyond the inherited distal tubular acidosis, our findings also challenge the existing paradigm on the exclusive role of PCs and offer the new view that ICs and PCs are both critical in maintaining sodium balance, and hence, normal vascular volume.

RESULTS

Atp6v1b1$^{-/-}$ mice have an impaired ability to conserve Na^+, Cl^-, K^+, and water despite the absence of interstitial nephritis or nephrocalcinosis

To test whether the *Atp6v1b1*$^{-/-}$ mice have an impaired renal ability to conserve Na^+ and Cl^-, physiological blood and urine parameters were measured in *Atp6v1b1*$^{-/-}$ mice and their wild-type counterparts (*Atp6v1b1*$^{+/+}$) that were pair-fed either a normal (0.3% Na^+) or a Na^+-free diet (all data are summarized in Table S1). As shown in Figure 1, urinary excretion of Na^+ and Cl^- was similar in both groups when the animals were fed a normal diet. During the first 24-hr of NaCl restriction, *Atp6v1b1*$^{-/-}$ mice excreted more Na^+ (Figure 1A) and Cl^- (Figure 1B) than pair-fed wild-type mice. However, within 3 days of NaCl restriction, all mice reached steady state resulting in similar rates of Na^+ and Cl^- excretion in both genotypes. We also observed that *Atp6v1b1*$^{-/-}$, even when fed a normal salt diet, exhibited hallmarks of vascular dehydration as evident from increased plasma renin activity (Figure 1C) and plasma protein concentrations (45.7 ± 0.8 g/l in *Atp6v1b1*$^{+/+}$ n=10, vs. 50.2 ± 1.2 g/l in *Atp6v1b1*$^{-/-}$, n=9; p = 0.005) (Table S1). In addition, *Atp6v1b1*$^{-/-}$ mice exhibited lower systolic blood pressure (112.4 ± 2.8 mmHg in *Atp6v1b1*$^{+/+}$ vs. 95.4 ± 2.5 mmHg in *Atp6v1b1*$^{-/-}$, n=10 and 6, respectively; p<0.001). The development of marked secondary hyperaldosteronism in *Atp6v1b1*$^{-/-}$ mice subjected to NaCl restriction (Figure 1D) further suggests the presence of vascular dehydration in these animals. Taken together, these observations indicate that *Atp6v1b1*$^{-/-}$ mice have vascular dehydration and an impaired renal ability to conserve both Na^+ and Cl^-, and hence, that they have a salt-losing nephropathy.

Under basal conditions *Atp6v1b1*$^{-/-}$ mice exhibited a lower plasma K^+ concentration (Figure 1E) than control mice, but an inappropriately normal urinary excretion of K^+ (Figure 1F). Moreover, when animals were subjected to NaCl restriction (*i.e.*, under conditions of maximal stimulation of aldosterone), urinary excretion of K^+ in mutant animals was exacerbated and became higher, *i.e.*, inappropriate for hypokalemia, than in controls (Figure 1F), demonstrating a renal defect in K^+ conservation.

In addition, we noticed that *Atp6v1b1*$^{-/-}$ mice exhibited polyuria that was also dramatically magnified by salt restriction (Figure 1G). Figure 1H shows that urine produced by *Atp6v1b1*$^{-/-}$ mice had a lower osmolality (1160 ± 124 mOsmol/kg; n = 7) than that of wild-type mice (2151 ± 31 mOsmol/kg; n = 8) under a normal Na^+ diet. Na^+-depleted diet had no significant effect on urine osmolalities (2437 ± 236 mOsmol/kg; n = 8 wild-type mice and 971 ± 211 mOsmol/kg; n = 6 knock-out mice).

These experiments demonstrate that *Atp6v1b1* disruption leads to a complex tubulopathy, which recapitulates major features observed in some patients suffering from classic type I dRTA and which have been attributed to chronic interstitial nephritis. However, careful examination by light microscopy of kidney sections from *Atp6v1b1*$^{-/-}$ mice demonstrated the absence of interstitial nephritis, and no evidence of microscopic nephrocalcinosis was found in sections examined after Von Kossa staining (Figure S1).

Atp6v1b1 gene deletion inhibits ENaC in the CCD but not in the MCD

Atp6v1b1 disruption leads to markedly reduced proton pump activity in α-ICs (19, 20) and possibly also in β-ICs. Pharmacological blockade of the pump has been shown to inhibit pendrin-dependent Cl^- absorption by CCDs (21). Therefore, we hypothesized that *Atp6v1b1* disruption should reduce the electroneutral NaCl transport system via β-ICs that we recently described and that requires normal pendrin activity (16). To test this hypothesis, Na^+ and Cl^- transepithelial fluxes (J_{Na} and J_{Cl}) were measured in CCDs isolated from *Atp6v1b1*$^{-/-}$ mice fed either a normal or a low salt diet. In a previous study, we have shown that CCDs isolated from wild type mice fed a normal salt diet do not exhibit any detectable transport activity, whereas CCDs isolated from mice fed a salt depleted diet absorb NaCl through the epithelial Na^+ channel ENaC in principal cells and the pendrin/Ndcbe transport system in intercalated cells (16). As *Atp6v1b1*$^{-/-}$ mice fed a normal salt diet exhibited higher plasma renin activity (similar to that of wild type mice maintained on salt depleted diet for six days), one could have expected their CCDs to absorb NaCl as those from wild type mice maintained on a salt depleted diet. However, CCDs isolated from *Atp6v1b1*$^{-/-}$ mice were not able to absorb Na^+ or Cl^- (J_{Na} = -4.23 ± 4.43 and J_{Cl} = -4.05 ± 6.92 pmol/min/mm ; n = 5). This was also the case for CCDs isolated from *Atp6v1b1*$^{-/-}$ mice fed a salt depleted diet (Figure 2A). J_{Na} and J_{Cl} were approximately ten-fold less than in *Atp6v1b1*$^{+/+}$ mice fed a salt depleted diet. These results suggest that in addition to impairing electroneutral Na^+ absorption through ICs, *Atp6v1b1* disruption also inhibits Na^+ absorption mediated by ENaC through the neighboring principal cells. Since ENaC is expressed exclusively in principal cells, *Atp6v1b1* disruption was not expected to affect directly electrogenic Na^+ absorption by CCD.

To dissect the mechanisms by which *Atp6v1b1* disruption impairs NaCl reabsorption in the CCD, we next performed semiquantitative immunoblotting to measure pendrin and ENaC protein abundance in the renal cortex of *Atp6v1b1*$^{-/-}$ mice under basal conditions. Figure 2B shows that abundances of both α-ENaC (left panel) and γ-ENaC (middle panel) were

approximately 50% lower in knock-out mice than in wild type mice. Pendrin protein level was reduced by 80% when compared to controls (Figure 2B, right panel). Data are summarized in Table 1. Taken together, our results demonstrate that *Atp6v1b1* disruption inhibits electroneutral NaCl absorption by reducing pendrin expression in β-IC, but also impairs principal cell function by decreasing ENaC expression and function. Of interest, mice with gene disruption of pendrin have been shown to exhibit similar alterations in ENaC abundance as *Atp6v1b1*$^{-/-}$ mice (22). We next studied the effects of *Atp6v1b1* disruption in the medullary collecting duct (MCD), a nephron segment that contains exclusively principal cells and α-ICs but does not have β-ICs. Figure 2C and Table 1 show that in the renal medulla, in contrast to our observations in the renal cortex, abundance of both α and γ subunits of ENaC were dramatically increased in knock-out mice, as expected from mice with secondary hyperaldosteronism. Unfortunately, we could not measure Na^+ fluxes in MCDs, as this segment is not easily accessible for *in vitro* microperfusion. Alternatively, we estimated total ENaC activity in *Atp6v1b1*$^{-/-}$ mice by assessing the effects of an acute injection of amiloride (1.45 mg/kg of body weight) on urinary excretion of Na^+. Amiloride injection significantly increased urine Na^+ excretion in both genotypes and was only slightly less effective in *Atp6v1b1*$^{-/-}$ mice than in controls (Figure 2, panel D) indicating that ENaC-dependent Na^+ absorption in the distal nephron is slightly lower in *Atp6v1b1*$^{-/-}$ mice. These results suggest that decreased ENaC activity in the CNT/CCD is almost fully compensated by increased ENaC activity in the MCD. In summary, our results show that β-IC dysfunction consecutive to *Atp6v1b1* disruption inhibits NaCl absorption and impairs the sensitivity of principal cells to renin-angiotensin-aldosterone system activation in the CCD, while principal cells in the MCD have a normal response to hyperaldosteronism. Our results strongly suggest that a factor originating from the β-IC locally reduces ENaC activity in the cortex.

Atp6v1b1-null mice have increased expression of the large conductance calcium-activated potassium channel in collecting ducts.

In the connecting tubule and the collecting duct, K^+ secretion occurs through two types of apical K^+ channels: the renal outer medullary K^+ (ROMK) channel and the large conductance calcium-activated K^+ channel (BKCa).

Movement of K^+ across the apical membrane through selective apical K^+ channels required a favorable electrical driving force, which is provided by electrogenic reabsorption of Na^+ through ENaC. Since ENaC was found up-regulated in the MCD (Figure 2C), we tested

whether K^+ leak could occur through ROMK in the MCD of *Atp6v1b1*$^{-/-}$ mice. We next analyzed the abundance of ROMK protein in the medulla. As detailed in supplementary information (Figure S2, panel A), in the medulla, anti ROMK antibody detected a triplet around 37 kDa in which the upper band was shown to correspond to the molecular form of ROMK expressed exclusively in the collecting duct. We found that ROMK protein abundance was markedly increased in MCD from *Atp6v1b1*$^{-/-}$ mice (Table 1 and Figure S2, panel B). The large conductance calcium-activated K^+ channel BKCa mediates the flow-induced K^+ secretion in the collecting duct (23). Elevated urinary flow in *Atp6v1b1*$^{-/-}$ mice may activate BKCa channels and K^+ secretion. When assessed by immunoblotting, the protein level of the α subunit of the BKCa channel was increased by 1.6 and 2.6-fold in cortical and medullary samples from *Atp6v1b1*$^{-/-}$ mice, respectively (Figure 3, panel A and Table 1). These results show increases in K^+ channels expression in *Atp6v1b1*$^{-/-}$ mice, which parallel up-regulation of ENaC in the MCD.

Expression of AQP2 was dramatically decreased in collecting ducts of Atp6v1b1-null mice

Accumulation of aquaporin 2 (AQP2) in the apical plasma membrane increases water permeability of the collecting duct allowing water to be reabsorbed from the collecting duct lumen and increasing the concentration of the urine. Immunoblotting studies showed that renal medulla AQP2 protein level was dramatically reduced (by 70%) in *Atp6v1b1*$^{-/-}$ mice as compared with control mice (Figure 3B and Table 1). In the cortex, AQP2 protein level in *Atp6v1b1*$^{-/-}$ mice was decreased by 40 % (Figure S3, panel A and Table 1). These results were confirmed by immunofluorescence on kidney sections (Figure 3, panel C and Figure S3, panel B). These results suggest that water loss in *Atp6v1b1*$^{-/-}$ mice is likely a consequence of downregulation of AQP2.

Abnormal prostaglandin E_2 release impairs ENaC regulation in CCDs

Increased urine prostaglandin E_2 (PGE_2) excretion is often associated with salt and water losing nephropathies (24). The collecting duct is a major site of PGE_2 synthesis in the kidney, where PGE_2 inhibits both salt and water absorption (25, 26). We next measured PGE_2 excretion in the urine of *Atp6v1b1*$^{-/-}$ mice and their controls. Urinary PGE_2 was increased 2 fold in *Atp6v1b1*$^{-/-}$ mice (Figure 4A). To test whether principal cell dysfunction in our model could arise from an abnormal PGE_2 release, we treated *Atp6v1b1*$^{-/-}$ mice with indomethacin, an unselective inhibitor of cyclooxygenases, the enzyme responsible for prostaglandin generation. Urinary PGE_2 excretion of *Atp6v1b1*$^{-/-}$ mice was significantly decreased 24 hours

after the first injection of indomethacin (5 mg/kg b.w./day) and a maximal 60 % decrease was observed after 2 days. At day 2, indomethacin improved the polyuria and normalized urine osmolality (Table 2), and abolished the difference in plasma potassium concentration (4.10 ± 0.07 mM, n=25 *Atp6v1b1*$^{+/+}$ mice vs 3.54 ± 0.08 mM, n=24 *Atp6v1b1*$^{-/-}$ mice, without indomethacin treatment; $p<0.0001$ and 4.11 ± 0.07 mM, n=24 *Atp6v1b1*$^{+/+}$ mice vs 3.90 ± 0.09 mM, n=27 *Atp6v1b1*$^{-/-}$ mice, following indomethacin treatment; NS). Urinary Na^+ and K^+ excretions also decreased in response to indomethacin treatment in mutant mice (Table 2). Indomethacin reduced differences in plasma renin activity (PRA) between wild type and mutant mice (PRA in *Atp6v1b1*$^{-/-}$ mice was 6 fold that of *Atp6v1b1*$^{+/+}$ mice, without indomethacin, and only 2.3 fold that of *Atp6v1b1*$^{+/+}$ mice, with indomethacin, $p=0.047$) and abolished the difference in hematocrit (41 ± 1 %, n=38 *Atp6v1b1*$^{+/+}$ mice vs. 44 ± 1 %, n=40 *Atp6v1b1*$^{-/-}$ mice, without indomethacin treatment; $p<0.01$ and 40 ± 1 %, n=16 *Atp6v1b1*$^{+/+}$ mice vs. 39 ± 2 %, n=17 *Atp6v1b1*$^{-/-}$ mice, following indomethacin treatment; NS). Indomethacin treatment had no significant effect in wild type mice. Western blot analyses shown in Figures 5A and 5C indicate that protein abundance for α– and γ-ENaC in cortical homogenates was no longer down-regulated, and was even slightly higher for γ-ENaC in treated *Atp6v1b1*$^{-/-}$ mice when compared to control mice. In contrast, pendrin expression remained very low (Table 1) in treated *Atp6v1b1*$^{-/-}$ mice. Expression of α– and γ-ENaC in the medullary collecting duct was still increased in treated *Atp6v1b1*$^{-/-}$ mice (Figures 5B and 5D) when compared to control mice as well as the expression of ROMK (Table 1). These results demonstrate that abnormal ENaC regulation in the CCD is due to a disturbance in PGE_2 paracrine signaling, whereas the reduction of pendrin is a direct consequence of proton pump dysfunction. Expression of AQP2 was also normalized by indomethacin treatment in both cortical and medullary samples (Figures 5E and 5F and Table 1). After indomethacin treatment, the expression of the α subunit of the BKCa channel was not different from that of control mice in both cortical and medullary samples (Figures 5G and 5H and Table 1). All densitometric analyses of immunoblots are summarized in Table 1. Taken together, these results indicate that renal K^+ loss in *Atp6v1b1*$^{-/-}$ mice is likely a consequence of activation of flow-activated BKCa potassium channels.

Inactivation of the basolateral H^+-ATPase induced ATP dependent prostaglandins E2 release by the cortical collecting duct

The preceding experiments suggest that PGE_2 reduced ENaC activity in CCD principal cells. To get a better insight into the mechanism by which PGE_2 regulates ENaC function in CCD principal cells, we measured PGE_2 release into the tubular fluid in freshly isolated microperfused wild type CCDs in response to pharmacologic inhibition of basolateral H^+-ATPases in β-ICs using the previously established PGE_2 biosensor technique (27, 28). We used HEK cells overexpressing the calcium-coupled PGE_2 receptor EP1 as PGE_2 biosensors by loading them with Fluo-4/Fura Red to measure cytosolic calcium and positioning them in direct contact with the tubular fluid (Figure 6A). As shown in Figure 6B, addition of bafilomycin A1 to the bathing solution inhibiting basolateral H^+-ATPases in β-ICs caused significant elevation in HEK-EP1 biosensor cell calcium indicating luminal PGE_2 release. The selective EP1 receptor inhibitor SC51322 added to the luminal perfusate blocked bafilomycin-induced biosensor responses indicating PGE_2 specificity (Figure 6B).

Luminal ATP via activation of P2Y2 receptors is known to mediate inhibition of Na^+ absorption via ENaC in mouse CCD (29, 30). Recent studies have shown that local ATP can act either directly or via a signaling cascade that involves generation of active prostanoids, particularly PGE_2 (31-33), exerting natriuretic effects on the CCD. We thus tested the effect of the addition of the purinergic (ATP) receptor blocker suramin to the tubular perfusate and showed that bafilomycin-induced PGE_2 release was prevented by suramin (Figure 6B). Similarly, addition of the ATP scavenger apyrase (50 U/ml) to the tubular perfusate abolished PGE_2 biosensor responses consistent with its dependence on luminal ATP release (Figure 6B). Of note, as PGE_2, urinary ATP excretion was increased by 3.1 fold in *Atp6v1b1*$^{-/-}$ mice (Figure 4). Daily injection of indomethacin to *Atp6v1b1*$^{-/-}$ mice for two days, which normalized ENaC expression in the cortex (Figures 5A and 5C), had no significant effect on urinary ATP excretion (0.36 ± 0.12 pmol/min before vs 0.54 ± 0.20 pmol/min after indomethacin injection, N= 7) while decreasing PGE_2 excretion by 60%. These results suggest that ATP had no direct effect on ENaC expression but rather acted through PGE_2 generation in our model.

When CCDs were loaded with the calcium-sensitive ratiometric fluorophore pair Fluo-4 and Fura Red, the addition of bafilomycin to the bathing solution caused significant elevations in CCD $[Ca^{2+}]_i$, most significantly in ICs (Figure 6C). Suramin added to the tubular perfusate completely abolished the effects of bafilomycin (Figure 6D). These experiments evidence a significant intracellular calcium elevation in ICs, which reflects activation of luminal purinergic receptors in response to inactivation of the basolateral H^+-ATPase.

Overall, inhibition of basolateral H^+-ATPase in β-ICs leads to ATP release, which then triggers PGE_2 release by acting on luminal calcium-coupled purinergic P2 receptors, presumably P2Y2 receptors, the main luminal P2 receptor subtype expressed in the distal nephron.

DISCUSSION

Type 1 dRTA is associated with a salt- and potassium-losing nephropathy that can lead to renal hypokalemia and dehydration (9, 10). dRTA is also almost invariably complicated by a marked hypercalciuria resulting in kidney stones, bone demineralization, nephrocalcinosis, and ultimately chronic renal failure. Mice with disruption of the *Atp6v1b1* gene encoding the B1 subunit of the H^+-ATPase develop an abnormal response to an acid-load (19), which is the direct consequence of impaired proton secretion as expected from dysfunction of α-ICs. Our current results demonstrate that *Atp6v1b1* deficient mice, like patients with severe type I dRTA, have a salt losing nephropathy that leads to severe vascular dehydration when the animals are fed a NaCl-depleted diet. However, in the absence of nephrocalcinosis, this cannot be attributed solely to chronic interstitial nephritis but instead reflects abnormal NaCl handling by renal epithelial cells. In a previous study (16), we showed that CCDs isolated from mice with secondary hyperaldosteronism absorb Na^+ through ENaC in principal cells and through the Na^+-driven Cl^-/HCO_3^- exchanger NDCBE in intercalated cells. Cl^- absorption has been shown to occur in β-ICs through the Na^+-independent Cl^-/HCO_3^- exchanger pendrin (18, 34). Here, we demonstrate that, despite marked hypovolemia, CCDs isolated from *Atp6v1b1* deficient mice did not absorb NaCl, indicating that ENaC and NDCBE/pendrin activities are both impaired. Accordingly, expressions of pendrin, α- and γ-ENaC were decreased in the cortex of *Atp6v1b1* deficient mice. Reduction in protein expression as assessed by immunoblotting of renal cortex likely reflects changes in ENaC and pendrin expression in the CNTs as well. In contrast, in the renal medulla, protein abundances of both α- and γ-ENaC were dramatically increased as expected in hypovolemic animals. In vivo injection of amiloride further shows that global ENaC activity was only slightly altered in these mice, indicating that increased ENaC activity in the MCD almost fully compensated for decreased ENaC activity in the CNT/CCD of *Atp6v1b1*$^{-/-}$ mice. We conclude that β-IC dysfunction consecutive to *Atp6v1b1* disruption impairs the sensitivity of principal cells to renin-angiotensin-aldosterone system activation in the CCD, while principal cells in the MCD have a normal response to hyperaldosteronism.

Unlike human dRTA patients, *Atp6v1b1* deficient mice do not develop spontaneous acidosis. It has been shown that the B2 subunit, which is normally co-expressed with the B1 subunit in intercalated cells, compensates for the lack of the B1 subunit of the H^+-ATPase in

α-ICs and that its activity is sufficient to maintain acid-base homeostasis in *Atp6v1b1*$^{-/-}$ mice under basal conditions but not in conditions of acid load (20, 35) or stimulation of angiotensin II (36). Our data showing no electroneutral NaCl transport in the CCD of *Atp6v1b1*$^{-/-}$ mice suggested that the B2 isoform is not capable of compensating for the absence of B1 in β-ICs under all circumstances (normal and low salt diet), conditions that may require angiotensin II mediated regulation of H^+-ATPases.

Our results provide an explanation for hypokalemia in patients suffering from type 1 dRTA. K^+ is freely filtered at the glomerulus and is almost totally reabsorbed by the proximal tubule and the loop of Henle. The amount of K^+ excreted by the kidney is then determined by mechanisms beyond the early distal tubule, where either reabsorption or secretion of K^+ can occur. The two main mechanisms identified yet that account for K^+ secretion in the distal nephron are the small conductance K^+ channel ROMK and the large conductance, calcium-activated potassium channel BK (BKCa) (37). Apical ROMK channels are expressed in principal cells and K^+ secretion through ROMK channels depends on electrogenic Na^+ transport. BK channels have been primarily detected in apical membrane of ICs (38, 39), where basolateral Na-K-2Cl cotransporters (40, 41) may provide a mechanism for K^+ uptake, thereby allowing K^+ secretion through these cells. It is unlikely that K^+ secretion occurs through excessive activity of ROMK in CCD of *Atp6v1b1*$^{-/-}$ mice since ENaC activity in this tubule segment is blocked, as indicated by our microperfusion data (see figure 2A). Upregulation of ENaC in the OMCD of *Atp6v1b1*$^{-/-}$ mice is expected to drive excessive K^+ secretion through ROMK. High luminal flow rates are known to enhance K^+ secretion due to activation of BKCa channels (23). Thus, elevated urinary flow in mutant mice probably activates BKCa potassium channels and K^+ secretion. In line with this hypothesis, we found that BKCa expression was increased in mutant mice and that a reduction of urinary flow in *Atp6v1b1*$^{-/-}$ mice by indomethacin normalized expression level of BKCa and decreased urinary K^+ excretion in *Atp6v1b1*$^{-/-}$ mice. This data also indicates that PGE_2, which antagonizes the actions of vasopressin in the distal nephron (26), is responsible for the dramatic decreased expression of the AQP2 water channel seen in *Atp6v1b1*$^{-/-}$ mice and hence their urinary concentration defect.

Our findings showing differential regulation of ENaC in cortical connecting tubule/collecting duct system and medullary collecting duct suggest that ENaC expression and activity in the CNT and the CCD are modulated by β-ICs. This is in line with recent studies showing that pendrin-null mice have an impaired ability to conserve Na^+ during dietary NaCl restriction and reduced ENaC expression (22). It has been shown that pendrin

can increase ENaC abundance and function in part by increasing luminal HCO_3 concentration and/or pH (42). However, it is unlikely that this mechanism can fully explain reduced cortical ENaC activity and expression observed in *Atp6v1b1* deficient mice. In fact, *Atp6v1b1*$^{-/-}$ mice exhibited much higher urinary pH than control mice (6.6 ± 0.03 vs 5.8 ± 0.02, n=7 and 8 respectively, $p<0.0001$). Moreover, indomethacin, which decreased urinary PGE_2 excretion in *Atp6v1b1* deficient mice, normalized ENaC expression specifically in the renal cortex. Indomethacin also tended to decrease urinary Na^+ excretion in these mice, and reduced differences in plasma renin activity and hematocrit between wild type and mutant mice. Furthermore, we demonstrate that inactivation of the H^+-ATPase induces PGE_2 release by isolated microperfused CCD. Considering these data, and because PGE_2 has been repeatedly shown to decrease electrogenic Na^+ transport in isolated and microperfused CCDs (25, 26, 43), we propose that PGE_2 production has a primary role in downregulating ENaC expression and function in the CCD of *Atp6v1b1* deficient mice. This autocrine/paracrine function of PGE_2 in regulating Na^+ transport in the CCD has been recently evidenced in isolated and microperfused tubules by Flores et al. (44). The authors showed that indomethacin enhanced flow-stimulated Na^+ absorption in microperfused CCDs and concluded that flow-activated PGE_2 release inhibits Na^+ absorption. Opposing regulations of ENaC in the CCD and the MCD highlight the importance of this paracrine PGE_2 signaling in antagonizing the action of the renin–angiotensin–aldosterone-system on ENaC in the CCD.

The present studies demonstrate that PGE_2 release by isolated micropefused CCDs in response to the preferential inactivation of the basolateral H^+-ATPase requires activation of luminal G protein-coupled purinergic (ATP) receptor. Such ATP-induced PGE_2 release has been observed in other cell types including astrocytes (33), vascular smooth vessel cells (31) and inner medullary collecting duct cells (32).

In the mouse kidney, ATP-permeable hemichannel connexin 30 (Cx30), which has been localized solely to the apical membrane of β-ICs of the distal nephron (45), is involved in ATP release from the collecting duct cells (15, 28). More recently, pannexin 1 channels (Panx1), expressed at the apical membrane of ICs, has also been proposed to regulate ATP release as *Panx1* deficient mice excrete less ATP than their wild type littermates (15, 46). Thus, ATP released via Cx30 and/or Panx1 is theorically available for autocrine and paracrine signaling to intercalated and principal cells, respectively. The calcium coupled P2Y2 receptor is the main luminal P2 receptor subtype expressed in the distal nephron and was located in principal cells using confocal microscopy imaging (47). With calcium imaging experiments on isolated CCDs, we also evidence a strong intracellular calcium elevation in ICs in response

to the preferential inactivation of the basolateral H^+-ATPase, which was abolished in the presence of luminal suramin. These data strongly suggest that ICs themselves respond to purinergic signaling.

In the collecting duct, luminal ATP via activation of P2Y2 receptors inhibits Na^+ ENaC-dependent Na^+ transport (29, 30). Activation of purinergic P2 receptors also decreases AVP-induced water permeability and down-regulates AQP2 (48, 49). Our experiments showing that indomethacin treatment restores normal protein levels of ENaC and AQP2 in the renal cortex of *Atp6v1b1* deficient mice but has no effect on urinary ATP excretion suggests that ATP acts through PGE_2 generation in CCDs of *Atp6v1b1* deficient mice. However, we cannot rule out the possibility of a direct effect of ATP on ENaC activity through a reduction in channel open probability.

The effects of PGE_2 are mediated by a distinct class of G protein-coupled receptors referred to as E-prostanoid (EP) receptors. Among the three EP receptor subtypes that have been localized in the cortical collecting duct (e.g., EP1, EP3 and EP4 receptors), activation of EP1 receptors by basolateral PGE_2 increases intracellular calcium levels and inhibits Na^+ absorption in the *in vitro* microperfused cortical collecting duct (25). Basolateral PGE_2 through G_i protein coupled EP3 receptors inhibits vasopressin-stimulated water permeability of this epithelium (26). PGE_2 produced by the cortical collecting cells and released across the basolateral membrane of these cells may enter the bloodstream by diffusing into the peritubular capillaries and could potentially circulate and activate their remote EP3 receptors in the medulla. Alternatively, activation of the renin-angiotensin-alsosteron system has been suggested to induce PGE_2 synthesis in the renal medulla (50). In addition to this well-known basolateral effect of PGE_2, there is evidence for luminal prostaglandin receptors in the cortical collecting duct, activation of which suppresses ENaC mediated Na^+ transport (43). As indicated by our biosensor experiments, which measured luminal PGE_2, PGE_2 release also occurs through luminal cell membranes of the CCD. Luminal PGE_2 has been reported to increase cAMP production in culture CCD cells (51, 52), suggesting that the effects of luminal PGE_2 are mediated by Gs protein coupled EP receptors. EP2 and EP4 are coupled to the Gs protein and signal by increasing intracellular cAMP levels, but only the EP4 receptor has been localized in the cortical collecting duct (53). Thus, PGE_2 release through luminal and basolateral cell membranes of the CCD may inhibit Na^+ transport through activation of EP1 and EP4 receptors and water transport through EP3 receptor activation.

The importance of the intratubular paracrine factor ATP as a regulator of electrolytes and water balance in the distal nephron is emerging (15). In contrast to aldosterone, which is a

powerful stimulatory factor of Na^+ absorption through PCs, ATP as PGE_2 exert an inhibitory effect on Na^+ absorption. The importance of these paracrine factors in blood pressure regulation is highlighted by previous studies showing that disruption of the purinergic P2Y2 receptor or the microsomal prostaglandin E synthase 1, a key enzyme in PGE_2 synthesis, leads to salt sensitive hypertension in mice (54, 55). In the present study, we identified β-ICs as an important site of ATP release, which triggers through P2Y2 receptor activation the local production and release of PGE_2. We also show that β-ICs can down-regulate ENaC in the neighboring PCs through this PGE_2/ATP signaling. Genetic ablation of connexin 30 in mouse causes salt-sensitive increase in blood pressure (28). Impairment of this paracrine signaling originating from β-ICs may be involved in the pathogenesis of several forms of salt sensitive hypertension.

This paracrine ATP/PGE_2 signaling originating from β-ICs for modulating Na^+ absorption in the CCD seems well adapted to acutely modulate Na^+ absorption in response to tubular NaCl overloading. Indeed, the distal nephron is challenged daily by variations in tubular fluid NaCl concentration as a direct consequence of dietary salt intake. Urinary ATP levels have been shown to increase with dietary Na^+ intake (56, 57). We propose a paradigm where β-ICs would sense the increase in NaCl delivery to the distal nephron and in turn release ATP/PGE_2 to decrease Na^+ absorption by adjacent PCs. We have reported that pendrin is primarily regulated in response to chronic changes in Cl^- balance (i.e., pendrin expression is decreased when Cl^- excretion increases) (58, 59). Thus, coordinated inhibition of Na^+ and Cl^- absorption through both PCs and ICs will allow the body to get rid of the excess of NaCl brought about by the diet.

In conclusion, we demonstrate that impaired renal sodium and potassium conservation observed in type 1 (or pump-defect type) dRTA is not the consequence of acidosis or of chronic interstitial nephritis, but is instead the consequence of the dysfunction of the proton pump in the β-IC. We propose a new paradigm where dysfunction of the proton pump in α-IC results in an acidification defect while dysfunction of the pump in β–IC is responsible for renal loss of NaCl, K^+ and water (figure 7). In light of the present study, it would be of interest to measure urinary prostaglandin excretion in human dRTA patients in future studies and to determine whether indomethacin treatment would improve dehydration and hypokalemia in these patients.

METHODS

Animals: *Atp6v1b1*$^{-/-}$ mice were kindly provided by Lifton R (Yale University, New Haven, CT, USA). Mice heterozygous for *Atp6v1b1* gene disruption were crossed, and wild-type (*Atp6v1b1*$^{+/+}$) and homozygous knockout mice (*Atp6v1b1*$^{-/-}$) were genotyped in their offspring by PCR of tail biopsies. In all experiments, controls consisted of wild type littermates.

Physiological studies: All experiments were performed using age- and sex-matched *Atp6v1b1*$^{+/+}$ and *Atp6v1b1*$^{-/-}$ littermates mice (3-5 month-old). For urine collection, mice were housed in metabolic cages (Techniplast). Mice were given deionized water ad libitum and pair-fed with standard laboratory chow containing 0.3% of sodium (INRA). They were first allowed to adapt for 3-5 days to the cages. At steady state, urine collection was performed daily under mineral oil in the urine collector for electrolyte measurements. Mice were then switched to a NaCl free diet (INRA). After the switch, urines were collected for the 6 first hours and for the subsequent 18 hours, and then each 24 hours for 7 days. Urine creatinine (modified kinetic Jaffé colorimetric method) was measured with a Konelab 20i auto-analyzer (Thermo Electron Corporation). Urinary chloride was measured with a DL 55 titrator (Mettler Toledo). Urinary Na^+ and K^+ were measured by flame photometry (IL943, Instruments Laboratory). Urine osmolalities were measured with a freezing point osmometer (Roebling). Plasma renin concentration was determined by radioimmunoassay of angiotensin I generated by incubation of the plasma at pH 8.5 in the presence of an excess of rat angiotensinogen (60). Urine aldosterone was measured by RIA (DPC Dade Behring). Urinary prostaglandin E_2 was measured by EIA (Prostaglandin E_2 EIA kit, Cayman chemicals). Urinary ATP was measured on diluted urines with the FLAA kit from Sigma. Blood collection by tail incision on anesthetized mice by peritoneal injection of a mixture (0.1ml/g body weight) of ketamine (Imalgene®, Rhône Mérieux; 10%) and xylazine (Rompun®, Bayer AG; 5%) was performed for K^+ measurement with an ABL 77 pH/blood-gas analyzer (Radiometer). Blood gases analyses were performed by retro-orbitary punction, and pH, PCO_2, PO_2, Na^+ and Cl^- were measured with an ABL 77 pH/blood-gas analyzer (Radiometer). Blood bicarbonate concentration was calculated from the measured values using the Henderson-Hasselbach equation.

For indomethacin treatment, indomethacin (Sigma) dissolved in ethanol (10 % volume) and saline was injected intraperitonealy once a day for up to 6 days (5 mg/kg b.w./day). Urines were collected daily and keep frozen at -80°C.

Blood-pressure measurements in conscious mice. Systolic blood pressure was measured in conscious mice fed a normal salt diet using a computerized tail-cuff system after 1 week of daily training, as described elsewhere (61). Then at least 10 measurements were performed every day for at least seven consecutive days. Only the last four days were kept for analyses. If the variability of the measurements made in a single day exceeded the SD by more than 20%, this day was discarded and replaced by an additional day of measurement. This method has been extensively validated and correlates well with direct measurements of intra-arterial pressure (61).

Immunoblot analyses: Animals were sacrificed with ketamine and xylazine (0.1 and 0.01 $mg \cdot g$ of body $weight^{-1}$, respectively). Kidneys were removed and cut into 5-mm slices and the cortex and medulla were excised under a stereoscopic microscope and placed into ice-cold isolation buffer (250 mM sucrose, 20 mM Tris-Hepes, pH 7.4) containing protease inhibitors in μg/ml: 4 aprotinin, 4 leupeptin, 1.5 pepstatin A and 28 4-(2- aminoethyl)-benzenesulfonyl fluoride (AEBSF). Minced renal tissues were homogenized in a Dounce homogenizer (pestle A, 5 passes) followed by 10 passes through a Teflon-glass homogenizer rotating at 1000 rpm. The homogenate was centrifuged at 1000 g for 10 min (rotor JS-13.1, Beckman), and the supernatant was centrifuged at 360,000 g for 40 min at 4°C (rotor 70.1 Ti, Beckman). The pellet was resuspended in isolation buffer. Protein contents were determined using the Bradford protein assay (microBradford, Bio Rad Laboratories).

Membrane proteins were solubilized in SDS-loading buffer (62.5 mM Tris HCl, pH 6.8, 2% SDS, 100 mM dithiotreitol, 10% glycerol and bromophenol blue), incubated at room temperature for 30 min. Electrophoresis was initially performed for all samples on 7.5% polyacrylamide minigels (XCell *SureLock* Mini-cell, Invitrogen Life Technologies), which were stained with Coomassie blue to provide quantitative assessment of loading (Supplementary figure S4), as previously described (58). For immunoblotting, proteins were transferred electrophoretically (XCell II Blot Module, Invitrogen Life Technologies) for 1.5 h at 4°C from unstained gels to nitrocellulose membranes (Amersham) and then stained with 0.5% Ponceau S in acetic acid to check uniformity of protein transfer onto the nitrocellulose membrane. Membranes were first incubated in 5% nonfat dry milk in phosphate-buffered

saline, pH 7.4 (PBS) for 1 h at room temperature to block nonspecific binding of antibody, followed by overnight at 4°C with the primary antibody (anti-Pendrin 1:10000; anti AQP2 1:100; anti α-ENaC 1:10000 ; anti γ-ENaC 1:30000; anti ROMK 1:2000 ; anti BKCa α subunit 1 :500 ; anti β-actin 1:500000) in PBS containing 1% nonfat dry milk. After four 5 min washes in PBS containing 0.1% Tween-20, membranes were incubated with 1:10000 dilution of goat anti-rabbit IgG (Bio-Rad) or horse anti-goat IgG (Vector Laboratories, Burlingame, CA) conjugated to horseradish peroxidase in PBS containing 5% nonfat dry milk for 2 hours at room temperature. Blots were washed as above, and luminol-enhanced chemiluminescence (ECL, Perkin Elmer Life Science Products) was used to visualize bound antibodies before exposure to Hyperfilm ECL (Amersham). The autoradiography was digitized with the use of a laser scanner (Epson Perfection 1650, Epson), and quantification of each band was performed by densitometry using NIH Image software. Densitometric values were normalized to the mean for the control group that was defined as 100% and results were expressed as mean ± S.E.

Antibodies against α and γ subunits of ENaC were a kind gift from J Loffing (University of Zurich, Zurich, Switzerland). Antibody against α-ENaC was raised against the N-terminus of mouse α-ENaC (MLDHTRAPELNLDLDLDVSNC)(62). Antibody against γ–ENaC was described elsewhere (63). Antibodies against pendrin (64) were a gift from P Aronson (Yale University, New Haven, CN). Antibodies against aquaporin 2 used for immunoblotting were purchased from Santa Cruz Biotechnology (Santa Cruz, CA). Antibodies againt ROMK and BK α subunit were purchased from Alomone labs. Antibodies against β-actin were purchased from Abcam.

Immunofluorescence labeling on kidney tissue: Mice kidneys were fixed in situ by perfusion of 4% paraformaldehyde in Phosphate Buffer Saline. Coronal kidney sections containing all kidney zones were then postfixed for 4–6 h at 4°C in 4% paraformaldehyde and then embedded in paraffin. Subsequently, 4-μm sections of the paraffin block were deparaffinized in toluene and rehydrated through graded ethanol. Rehydration was completed in Tris-buffered saline (TBS), pH 7.6. Slides were then placed in a plastic tank filled with Target Retrieval Solution (Dako) and heated 45 min in a water bath at 98°C. These steps unmasked antigens and allowed immunostaining of paraformaldehyde-fixed paraffin sections, as determined in preliminary experiments (not shown). To reduce nonspecific binding, sections were rinsed in TBS for 10 min and incubated with background-reducing buffer (Dako) for 20

min. Mice kidney sections were then labeled with the rabbit polyclonal AQP2 antibody as follows. Anti-AQP2 was applied for 1 h at room temperature. After three washes, sections were incubated with a 1:1000 dilution (in background-reducing buffer) of donkey anti-rabbit IgG coupled to Cy^{TM}3 (Jackson Immunoresearch Laboratories Inc) in TBS, 30 min at room temperature, followed by three TBS washes. Rabbit anti AQP2 antibodies (AQP2 H7661) were a gift from S Frische (Aarhus University, Aarhus, Denmark) and were used by De Seigneux et al. (65).

In vitro microperfusion of mouse CCDs and transepithelial ion fluxes measurement:

Kidneys were removed, and cut into 1 to 2 mm coronal slices that were transferred into a chilled dissection medium containing (in mM): 118 NaCl, 25 $NaHCO_3$, 2.0 K_2HPO_4, 1.2 $MgSO_4$, 2.0 calcium lactate, 1.0 sodium citrate, 5.5 glucose, and 12 creatinine, pH 7.4, and gassed with 95% O_2-5% CO_2. CCD segments were isolated from cortico-medullary rays under a dissecting microscope with a sharpened forceps. Because CCDs are highly heterogeneous, relatively short segments (0.45-0.6 mm) were dissected to maximize the reproducibility of the isolation procedure. In vitro microperfusion was performed as described by Burg et al. (66): isolated CCDs were rapidly transferred to a 1.2 ml temperature- and environmentally-controlled chamber, mounted on an inverted microscope, and then perfused and bathed initially at room temperature with dissection solution. The specimen chamber was continuously suffused with 95% O_2-5% CO_2 to maintain pH at 7.4. Once secure, the inner perfusion pipette was advanced, and the tubule was opened with a slight positive pressure. The opposite end of the tubule was then pulled into a holding collection pipette. In the holding collection pipette, 2 to 3 cm of water-saturated mineral oil contributed to maintain the tubule open at a low flow rate of perfusion. The perfusing and collecting end of the segment was sealed into a guard pipette using Dow-Corning 200 dielectric fluid (Dow Corning Corp.). The tubules were then warmed to 37°C and equilibrated for 20 minutes while the collection rate was adjusted to a rate of 2 nl/min. The length of each segment was measured using an eyepiece micrometer. Because CCDs from mice are frequently unstable and collapse rapidly, measurements were conducted during the first 90 minutes of perfusion. Usually, collections from 4 periods of 15 minutes were performed in which 25 to 30 nanoliters of fluid were collected. The volume of the collections was determined under water-saturated mineral oil with calibrated volumetric pipettes. For [Na^+] and [creatinine] measurements, 20 nl were required, while 2–3 nanoliters were used for [Cl^-] determinations.

[Na^+] and [creatinine] measurements were performed by HPLC and [Cl^-] was measured by

microcoulometry as previously described (16, 67, 68).

Creatinine was used as the volume marker, and therefore was added to the perfusion solutions (both perfusate and bath) at a concentration of 12 mM. The rate of fluid absorption (*J*v) was calculated as *J*v = (Vperf – Vcoll)/L, with Vperf = Crcoll/Crperf x Vcoll.

Crcoll and Crperf are the concentrations of creatinine in the collected fluid and perfusate, respectively. Vcoll is the collection rate at the end of the tubule. L is the length of the tubule.

For each collection, Na^+ flux (JNa) was calculated and reported to the length of the tubule (L): J_{Na} =[([Na]perf x Vperf)– ([Na]coll x Vcoll)] /L and $J_{Cl} = [([Cl]_{perf} \times V_{perf}) - ([Cl]_{coll} \times V_{coll})]/L$, where "perf" indicates perfusate and "coll" indicates collection fluid. Therefore, positive values indicate net absorption, whereas negative values indicate net secretion of the ion. For each tubule, the mean of the 4 collection periods was used.

Fluorescence microscopy: The $[Ca^{2+}]_i$ of HEK/EP1 biosensor cells was measured as described previously (27). On average, 3-4 HEK/EP1 biosensor cells were placed at the tubule exit, and almost all biosensor cells produced PGE_2-induced calcium elevations.

Statistics: Experimental results are summarized as mean ± SEM. All statistical comparisons were made by use of unpaired Student's *t* test (two-tailed) or by ANOVA followed by a Bonferroni's post-hoc test when appropriate. A *P* value less than 0.05 was considered significant.

Study approval: All the experimental procedures have been approved by the local ethic committee from University Pierre et Marie Curie (agreement Ce5/2010/053) and were performed in accordance with the *Guide for the Care and Use of Laboratory Animals* (NIH publication No.93-23, revised 1985) and with the French Government animal welfare policy (Agreement number RA024647151FR).

ACKNOWLEGMENTS

We thank Luciana Morla for technical assistance. Régine Chambrey and Dominique Eladari are funded by INSERM, by CNRS, by Transatlantic Network for Hypertension (TNH) from the Fondation Leducq, by grant “subvention de recherche 2010 AMGEN” from the Société de Néphrologie to RC, by grant subvention de recherche 2010 from the “association pour l’information et la recherche sur les maladies rénales génétiques (AIRG)” to RC, and by grants from ANR BLANC 2012-R13011KK to R.C. and ANR BLANC 2010-R10164DD to D.E. from l'Agence Nationale de la Recherche (ANR). Nicolas Cornière is funded by la Fondation pour la Recherche Médicale (DEA20100619499). Maximilien Jayat is funded by the CODDIM from the Region Ile de France. Some of these studies were funded by DK64324 and an American Heart Association Established Investigator Award to J.P.P. CAW is supported by a grant from the Swiss National Science Foundation (31003A_138143/1).

REFERENCES

1. Alper, S.L. 2002. Genetic diseases of acid-base transporters. *Annu Rev Physiol* 64:899-923.
2. Wagner, C.A., Devuyst, O., Bourgeois, S., and Mohebbi, N. 2009. Regulated acid-base transport in the collecting duct. *Pflugers Arch* 458:137-156.
3. Alper, S.L., Natale, J., Gluck, S., Lodish, H.F., and Brown, D. 1989. Subtypes of intercalated cells in rat kidney collecting duct defined by antibodies against erythroid band 3 and renal vacuolar H+-ATPase. *Proc Natl Acad Sci U S A* 86:5429-5433.
4. Wagner, C.A., Finberg, K.E., Breton, S., Marshansky, V., Brown, D., and Geibel, J.P. 2004. Renal vacuolar H+-ATPase. *Physiol Rev* 84:1263-1314.
5. Karet, F.E., Finberg, K.E., Nelson, R.D., Nayir, A., Mocan, H., Sanjad, S.A., Rodriguez-Soriano, J., Santos, F., Cremers, C.W., Di Pietro, A., et al. 1999. Mutations in the gene encoding B1 subunit of H+-ATPase cause renal tubular acidosis with sensorineural deafness. *Nat Genet* 21:84-90.
6. Smith, A.N., Skaug, J., Choate, K.A., Nayir, A., Bakkaloglu, A., Ozen, S., Hulton, S.A., Sanjad, S.A., Al-Sabban, E.A., Lifton, R.P., et al. 2000. Mutations in ATP6N1B, encoding a new kidney vacuolar proton pump 116-kD subunit, cause recessive distal renal tubular acidosis with preserved hearing. *Nat Genet* 26:71-75.
7. Bruce, L.J., Cope, D.L., Jones, G.K., Schofield, A.E., Burley, M., Povey, S., Unwin, R.J., Wrong, O., and Tanner, M.J. 1997. Familial distal renal tubular acidosis is associated with mutations in the red cell anion exchanger (Band 3, AE1) gene. *J Clin Invest* 100:1693-1707.
8. Karet, F.E., Gainza, F.J., Gyory, A.Z., Unwin, R.J., Wrong, O., Tanner, M.J., Nayir, A., Alpay, H., Santos, F., Hulton, S.A., et al. 1998. Mutations in the chloride-bicarbonate exchanger gene AE1 cause autosomal dominant but not autosomal recessive distal renal tubular acidosis. *Proc Natl Acad Sci U S A* 95:6337-6342.
9. Sebastian, A., McSherry, E., and Morris, R.C., Jr. 1971. Renal potassium wasting in renal tubular acidosis (RTA): its occurrence in types 1 and 2 RTA despite sustained correction of systemic acidosis. *J Clin Invest* 50:667-678.
10. Sebastian, A., McSherry, E., and Morris, R.C., Jr. 1976. Impaired renal conservation of sodium and chloride during sustained correction of systemic acidosis in patients with type 1, classic renal tubular acidosis. *J Clin Invest* 58:454-469.
11. Gill, J.R., Jr., Bell, N.H., and Bartter, F.C. 1967. Impaired conservation of sodium and potassium in renal tubular acidosis and its correction by buffer anions. *Clin Sci* 33:577-592.
12. Finberg, K.E., Wagner, C.A., Stehberger, P.A., Geibel, J.P., and Lifton, R.P. 2003. Molecular cloning and characterization of Atp6v1b1, the murine vacuolar H+ -ATPase B1-subunit. *Gene* 318:25-34.
13. Stehberger, P.A., Schulz, N., Finberg, K.E., Karet, F.E., Giebisch, G., Lifton, R.P., Geibel, J.P., and Wagner, C.A. 2003. Localization and regulation of the ATP6V0A4 (a4) vacuolar H+-ATPase subunit defective in an inherited form of distal renal tubular acidosis. *J Am Soc Nephrol* 14:3027-3038.
14. Royaux, I.E., Wall, S.M., Karniski, L.P., Everett, L.A., Suzuki, K., Knepper, M.A., and Green, E.D. 2001. Pendrin, encoded by the Pendred syndrome gene, resides in the

apical region of renal intercalated cells and mediates bicarbonate secretion. *Proc Natl Acad Sci U S A* 98:4221-4226.

15. Eladari, D., Chambrey, R., and Peti-Peterdi, J. 2011. A New Look at Electrolyte Transport in the Distal Tubule. *Annu Rev Physiol*.
16. Leviel, F., Hubner, C.A., Houillier, P., Morla, L., El Moghrabi, S., Brideau, G., Hatim, H., Parker, M.D., Kurth, I., Kougioumtzes, A., et al. 2010. The Na+-dependent chloride-bicarbonate exchanger SLC4A8 mediates an electroneutral Na+ reabsorption process in the renal cortical collecting ducts of mice. *J Clin Invest* 120:1627-1635.
17. Verlander, J.W., Hassell, K.A., Royaux, I.E., Glapion, D.M., Wang, M.E., Everett, L.A., Green, E.D., and Wall, S.M. 2003. Deoxycorticosterone upregulates PDS (Slc26a4) in mouse kidney: role of pendrin in mineralocorticoid-induced hypertension. *Hypertension* 42:356-362.
18. Wall, S.M., Kim, Y.H., Stanley, L., Glapion, D.M., Everett, L.A., Green, E.D., and Verlander, J.W. 2004. NaCl restriction upregulates renal Slc26a4 through subcellular redistribution: role in Cl- conservation. *Hypertension* 44:982-987.
19. Finberg, K.E., Wagner, C.A., Bailey, M.A., Paunescu, T.G., Breton, S., Brown, D., Giebisch, G., Geibel, J.P., and Lifton, R.P. 2005. The B1-subunit of the H(+) ATPase is required for maximal urinary acidification. *Proc Natl Acad Sci U S A* 102:13616-13621.
20. Paunescu, T.G., Russo, L.M., Da Silva, N., Kovacikova, J., Mohebbi, N., Van Hoek, A.N., McKee, M., Wagner, C.A., Breton, S., and Brown, D. 2007. Compensatory membrane expression of the V-ATPase B2 subunit isoform in renal medullary intercalated cells of B1-deficient mice. *Am J Physiol Renal Physiol* 293:F1915-1926.
21. Pech, V., Kim, Y.H., Weinstein, A.M., Everett, L.A., Pham, T.D., and Wall, S.M. 2007. Angiotensin II increases chloride absorption in the cortical collecting duct in mice through a pendrin-dependent mechanism. *Am J Physiol Renal Physiol* 292:F914-920.
22. Kim, Y.H., Pech, V., Spencer, K.B., Beierwaltes, W.H., Everett, L.A., Green, E.D., Shin, W., Verlander, J.W., Sutliff, R.L., and Wall, S.M. 2007. Reduced ENaC protein abundance contributes to the lower blood pressure observed in pendrin-null mice. *Am J Physiol Renal Physiol* 293:F1314-1324.
23. Satlin, L.M., Carattino, M.D., Liu, W., and Kleyman, T.R. 2006. Regulation of cation transport in the distal nephron by mechanical forces. *Am J Physiol Renal Physiol* 291:F923-931.
24. Hao, C.M., and Breyer, M.D. 2008. Physiological regulation of prostaglandins in the kidney. *Annu Rev Physiol* 70:357-377.
25. Guan, Y., Zhang, Y., Breyer, R.M., Fowler, B., Davis, L., Hebert, R.L., and Breyer, M.D. 1998. Prostaglandin E2 inhibits renal collecting duct Na+ absorption by activating the EP1 receptor. *J Clin Invest* 102:194-201.
26. Hebert, R.L., Jacobson, H.R., Fredin, D., and Breyer, M.D. 1993. Evidence that separate PGE2 receptors modulate water and sodium transport in rabbit cortical collecting duct. *Am J Physiol* 265:F643-650.
27. Peti-Peterdi, J., Komlosi, P., Fuson, A.L., Guan, Y., Schneider, A., Qi, Z., Redha, R., Rosivall, L., Breyer, M.D., and Bell, P.D. 2003. Luminal NaCl delivery regulates basolateral PGE2 release from macula densa cells. *J Clin Invest* 112:76-82.
28. Sipos, A., Vargas, S.L., Toma, I., Hanner, F., Willecke, K., and Peti-Peterdi, J. 2009. Connexin 30 deficiency impairs renal tubular ATP release and pressure natriuresis. *J Am Soc Nephrol* 20:1724-1732.

29. Lehrmann, H., Thomas, J., Kim, S.J., Jacobi, C., and Leipziger, J. 2002. Luminal P2Y2 receptor-mediated inhibition of Na+ absorption in isolated perfused mouse CCD. *J Am Soc Nephrol* 13:10-18.
30. Pochynyuk, O., Bugaj, V., Rieg, T., Insel, P.A., Mironova, E., Vallon, V., and Stockand, J.D. 2008. Paracrine regulation of the epithelial Na+ channel in the mammalian collecting duct by purinergic P2Y2 receptor tone. *J Biol Chem* 283:36599-36607.
31. Lin, C.C., Lin, W.N., Wang, W.J., Sun, C.C., Tung, W.H., Wang, H.H., and Yang, C.M. 2009. Functional coupling expression of COX-2 and cPLA2 induced by ATP in rat vascular smooth muscle cells: role of ERK1/2, p38 MAPK, and NF-kappaB. *Cardiovasc Res* 82:522-531.
32. Welch, B.D., Carlson, N.G., Shi, H., Myatt, L., and Kishore, B.K. 2003. P2Y2 receptor-stimulated release of prostaglandin E2 by rat inner medullary collecting duct preparations. *Am J Physiol Renal Physiol* 285:F711-721.
33. Xia, M., and Zhu, Y. 2011. Signaling pathways of ATP-induced PGE2 release in spinal cord astrocytes are EGFR transactivation-dependent. *Glia* 59:664-674.
34. Wall, S.M., Hassell, K.A., Royaux, I.E., Green, E.D., Chang, J.Y., Shipley, G.L., and Verlander, J.W. 2003. Localization of pendrin in mouse kidney. *Am J Physiol Renal Physiol* 284:F229-241.
35. Vedovelli, L., Rothermel, J.T., Finberg, K.E., Wagner, C.A., Azroyan, A., Hill, E., Breton, S., Brown, D., and Paunescu, T.G. 2013. Altered V-ATPase expression in renal intercalated cells isolated from B1 subunit-deficient mice by fluorescence-activated cell sorting. *Am J Physiol Renal Physiol* 304:F522-532.
36. Rothenberger, F., Velic, A., Stehberger, P.A., Kovacikova, J., and Wagner, C.A. 2007. Angiotensin II stimulates vacuolar H+ -ATPase activity in renal acid-secretory intercalated cells from the outer medullary collecting duct. *J Am Soc Nephrol* 18:2085-2093.
37. Hebert, S.C., Desir, G., Giebisch, G., and Wang, W. 2005. Molecular diversity and regulation of renal potassium channels. *Physiol Rev* 85:319-371.
38. Najjar, F., Zhou, H., Morimoto, T., Bruns, J.B., Li, H.S., Liu, W., Kleyman, T.R., and Satlin, L.M. 2005. Dietary K+ regulates apical membrane expression of maxi-K channels in rabbit cortical collecting duct. *Am J Physiol Renal Physiol* 289:F922-932.
39. Palmer, L.G., and Frindt, G. 2007. High-conductance K channels in intercalated cells of the rat distal nephron. *Am J Physiol Renal Physiol* 292:F966-973.
40. Ginns, S.M., Knepper, M.A., Ecelbarger, C.A., Terris, J., He, X., Coleman, R.A., and Wade, J.B. 1996. Immunolocalization of the secretory isoform of Na-K-Cl cotransporter in rat renal intercalated cells. *J Am Soc Nephrol* 7:2533-2542.
41. Liu, W., Schreck, C., Coleman, R.A., Wade, J.B., Hernandez, Y., Zavilowitz, B., Warth, R., Kleyman, T.R., and Satlin, L.M. 2011. Role of NKCC in BK channel-mediated net K(+) secretion in the CCD. *Am J Physiol Renal Physiol* 301:F1088-1097.
42. Pech, V., Pham, T.D., Hong, S., Weinstein, A.M., Spencer, K.B., Duke, B.J., Walp, E., Kim, Y.H., Sutliff, R.L., Bao, H.F., et al. 2010. Pendrin modulates ENaC function by changing luminal HCO3. *J Am Soc Nephrol* 21:1928-1941.
43. Ando, Y., and Asano, Y. 1995. Luminal prostaglandin E2 modulates sodium and water transport in rabbit cortical collecting ducts. *Am J Physiol* 268:F1093-1101.
44. Flores, D., Liu, Y., Liu, W., Satlin, L.M., and Rohatgi, R. 2012. Flow-induced prostaglandin E2 release regulates Na and K transport in the collecting duct. *Am J Physiol Renal Physiol* 303:F632-638.

45. McCulloch, F., Chambrey, R., Eladari, D., and Peti-Peterdi, J. 2005. Localization of connexin 30 in the luminal membrane of cells in the distal nephron. *Am J Physiol Renal Physiol* 289:F1304-1312.
46. Hanner, F., Lam, L., Nguyen, M.T., Yu, A., and Peti-Peterdi, J. 2012. Intrarenal localization of the plasma membrane ATP channel pannexin1. *Am J Physiol Renal Physiol* 303:F1454-1459.
47. Deetjen, P., Thomas, J., Lehrmann, H., Kim, S.J., and Leipziger, J. 2000. The luminal P2Y receptor in the isolated perfused mouse cortical collecting duct. *J Am Soc Nephrol* 11:1798-1806.
48. Kishore, B.K., Chou, C.L., and Knepper, M.A. 1995. Extracellular nucleotide receptor inhibits AVP-stimulated water permeability in inner medullary collecting duct. *Am J Physiol* 269:F863-869.
49. Wildman, S.S., Boone, M., Peppiatt-Wildman, C.M., Contreras-Sanz, A., King, B.F., Shirley, D.G., Deen, P.M., and Unwin, R.J. 2009. Nucleotides downregulate aquaporin 2 via activation of apical P2 receptors. *J Am Soc Nephrol* 20:1480-1490.
50. Zusman, R.M., and Keiser, H.R. 1977. Prostaglandin biosynthesis by rabbit renomedullary interstitial cells in tissue culture. Stimulation by angiotensin II, bradykinin, and arginine vasopressin. *J Clin Invest* 60:215-223.
51. Garcia-Perez, A., and Smith, W.L. 1984. Apical-basolateral membrane asymmetry in canine cortical collecting tubule cells. Bradykinin, arginine vasopressin, prostaglandin E2 interrelationships. *J Clin Invest* 74:63-74.
52. Sakairi, Y., Jacobson, H.R., Noland, T.D., and Breyer, M.D. 1995. Luminal prostaglandin E receptors regulate salt and water transport in rabbit cortical collecting duct. *Am J Physiol* 269:F257-265.
53. Jensen, B.L., Stubbe, J., Hansen, P.B., Andreasen, D., and Skott, O. 2001. Localization of prostaglandin E(2) EP2 and EP4 receptors in the rat kidney. *Am J Physiol Renal Physiol* 280:F1001-1009.
54. Facemire, C.S., Griffiths, R., Audoly, L.P., Koller, B.H., and Coffman, T.M. 2010. The impact of microsomal prostaglandin e synthase 1 on blood pressure is determined by genetic background. *Hypertension* 55:531-538.
55. Rieg, T., Bundey, R.A., Chen, Y., Deschenes, G., Junger, W., Insel, P.A., and Vallon, V. 2007. Mice lacking P2Y2 receptors have salt-resistant hypertension and facilitated renal Na+ and water reabsorption. *FASEB J* 21:3717-3726.
56. Mironova, E., Peti-Peterdi, J., Bugaj, V., and Stockand, J.D. 2011. Diminished paracrine regulation of the epithelial na+ channel by purinergic signaling in mice lacking connexin 30. *J Biol Chem* 286:1054-1060.
57. Stockand, J.D., Mironova, E., Bugaj, V., Rieg, T., Insel, P.A., Vallon, V., Peti-Peterdi, J., and Pochynyuk, O. 2010. Purinergic inhibition of ENaC produces aldosterone escape. *J Am Soc Nephrol* 21:1903-1911.
58. Quentin, F., Chambrey, R., Trinh-Trang-Tan, M.M., Fysekidis, M., Cambillau, M., Paillard, M., Aronson, P.S., and Eladari, D. 2004. The Cl-/HCO3- exchanger pendrin in the rat kidney is regulated in response to chronic alterations in chloride balance. *Am J Physiol Renal Physiol* 287:F1179-1188.
59. Vallet, M., Picard, N., Loffing-Cueni, D., Fysekidis, M., Bloch-Faure, M., Deschenes, G., Breton, S., Meneton, P., Loffing, J., Aronson, P.S., et al. 2006. Pendrin regulation in mouse kidney primarily is chloride-dependent. *J Am Soc Nephrol* 17:2153-2163.
60. Menard, J., and Catt, K.J. 1972. Measurement of renin activity, concentration and substrate in rat plasma by radioimmunoassay of angiotensin I. *Endocrinology* 90:422-430.

61. Ito, M., Oliverio, M.I., Mannon, P.J., Best, C.F., Maeda, N., Smithies, O., and Coffman, T.M. 1995. Regulation of blood pressure by the type 1A angiotensin II receptor gene. *Proc Natl Acad Sci U S A* 92:3521-3525.
62. Sorensen, M.V., Grossmann, S., Roesinger, M., Gresko, N., Todkar, A.P., Barmettler, G., Ziegler, U., Odermatt, A., Loffing-Cueni, D., and Loffing, J. 2013. Rapid dephosphorylation of the renal sodium chloride cotransporter in response to oral potassium intake in mice. *Kidney Int* 83:811-824.
63. Wagner, C.A., Loffing-Cueni, D., Yan, Q., Schulz, N., Fakitsas, P., Carrel, M., Wang, T., Verrey, F., Geibel, J.P., Giebisch, G., et al. 2008. Mouse model of type II Bartter's syndrome. II. Altered expression of renal sodium- and water-transporting proteins. *Am J Physiol Renal Physiol* 294:F1373-1380.
64. Knauf, F., Yang, C.L., Thomson, R.B., Mentone, S.A., Giebisch, G., and Aronson, P.S. 2001. Identification of a chloride-formate exchanger expressed on the brush border membrane of renal proximal tubule cells. *Proc Natl Acad Sci U S A* 98:9425-9430.
65. de Seigneux, S., Malte, H., Dimke, H., Frokiaer, J., Nielsen, S., and Frische, S. 2007. Renal compensation to chronic hypoxic hypercapnia: downregulation of pendrin and adaptation of the proximal tubule. *Am J Physiol Renal Physiol* 292:F1256-1266.
66. Burg, M., Grantham, J., Abramow, M., and Orloff, J. 1966. Preparation and study of fragments of single rabbit nephrons. *Am J Physiol* 210:1293-1298.
67. Chambrey, R., Kurth, I., Peti-Peterdi, J., Houillier, P., Purkerson, J.M., Leviel, F., Hentschke, M., Zdebik, A.A., Schwartz, G.J., Hubner, C.A., et al. 2013. Renal intercalated cells are rather energized by a proton than a sodium pump. *Proc Natl Acad Sci U S A*.
68. El Moghrabi, S., Houillier, P., Picard, N., Sohet, F., Wootla, B., Bloch-Faure, M., Leviel, F., Cheval, L., Frische, S., Meneton, P., et al. 2010. Tissue kallikrein permits early renal adaptation to potassium load. *Proc Natl Acad Sci U S A* 107:13526-13531.

FIGURE LEGENDS

Figure 1: Effects of dietary NaCl restriction and renal K^+ and water handling in *Atp6v1b1*$^{-/-}$ mice. A. Time course of renal excretion of Na^+ in *Atp6v1b1*$^{-/-}$ and *Atp6v1b1*$^{+/+}$ mice fed a normal salt diet and then switch to a NaCl restricted diet. B. Time course of renal Cl^- excretion. C. Plasma renin concentration was measured under a normal salt diet, or after 6 days of NaCl restriction. D. Time course of urinary excretion of aldosterone. E. Plasma [K^+] was measured in *Atp6v1b1*$^{-/-}$ and *Atp6v1b1*$^{+/+}$ mice fed a normal salt diet or after 6 days of NaCl restriction. F. Time course of renal K^+ excretion when animals used for measurements of plasma [K^+] shown in panel E were switched from normal to NaCl-restricted diet. G. Time course of urine output. H. Time course of urine osmolality. Data are presented as means ± S.E.; n = 8 for *Atp6v1b1*$^{+/+}$ and 7 for *Atp6v1b1*$^{-/-}$. Statistical significance was assessed by unpaired Student's t-test. * $p<0.05$, ** $p<0.01$ and ***$p<0.001$ vs. *Atp6v1b1*$^{+/+}$

Figure 2: Differential effects of *Atp6v1b1* disruption on the cortical and medullary collecting duct. A. Effects of *Atp6v1b1* disruption on NaCl transport in the cortical collecting duct. Na^+ (J_{Na}) and Cl^- (J_{Cl}) transepithelial fluxes were measured in CCDs isolated from *Atp6v1b1*$^{+/+}$ mice (white bars) or *Atp6v1b1*$^{-/-}$ mice (black bars) fed a salt depleted diet for two weeks before the experiments. Statistical significance was assessed by 2-tailed unpaired Student's *t* test. N= 5 to 7 tubules from different mice in each group. *$P<0.05$. ***$P<0.001$. B. Effects of *Atp6v1b1* disruption on ENaC and pendrin expression in the cortical collecting duct. α-ENaC (left), γ-ENaC (middle) and pendrin (right) protein abundance was assessed by western blot of protein extracted from the renal cortex of *Atp6v1b1*$^{-/-}$ (black bars) and *Atp6v1b1*$^{+/+}$ mice (white bars). C. Effects of *Atp6v1b1* disruption on ENaC expression in the medullary collecting duct. α-ENaC (left) and γ-ENaC (middle) protein abundance was assessed by Western blot of protein extracted from the renal medulla of *Atp6v1b1*$^{-/-}$ (black bars) and *Atp6v1b1*$^{+/+}$ (white bars) mice. For panels B and C, each lane was loaded with a protein sample from a different mouse. 15 μg and 5 μg proteins were loaded per gel lane in B and C, respectively. Equal loading was confirmed by parallel Coomassie-stained gels. The α-ENaC antibody recognized two bands at 90 and 100 kDa. Only the 90 kDa (arrow) was not detected in kidneys from α-ENaC knock-out mice and therefore quantified. The γ-ENaC antibody recognized a doublet band at 85-80 kDa and a large band centered around 70 kDa

(bracket). Bar graphs show summary of densitometric analyses of the summation of the doublet band (85 kDa) and the broad 70 kDa band. Statistical significance was assessed by unpaired Student's t-test. *P<0.05, **P<0.01, ***P<0.001 vs. *Atp6v1b1*$^{+/+}$. D. Effect of amiloride on urinary Na^+ excretion in *Atp6v1b1*$^{+/+}$ and *Atp6v1b1*$^{-/-}$mice. Urines were collected before and 6 hours after amiloride injection (1.45 mg/kg body weight) to *Atp6v1b1*$^{+/+}$ and *Atp6v1b1*$^{-/-}$mice. Statistical significance was assessed by One way *ANOVA*. *** P<0.001 and ** P<0.01 vs. basal state. * P<0.05, *Atp6v1b1*$^{-/-}$ vs *Atp6v1b1*$^{+/+}$ mice after amiloride injection.

Figure 3: BKCa and AQP2 protein expression assessed in *Atp6v1b1*$^{-/-}$ and *Atp6v1b1*$^{+/+}$ mice. A. Western blot for αBKCa on renal cortex (left) or renal medulla (right). Each lane was loaded with a protein sample from a different mouse. 15 μg and 5 μg proteins were loaded per gel lane for cortical samples and medullary samples, respectively. B. Western blot for AQP2 on renal medulla. Bracket and asterisk show the glycosylated 37 kDa and the unglycosylated 25 kDa forms of AQP2, respectively. Each lane was loaded with a protein sample from a different mouse. 5 μg proteins were loaded per gel lane. Equal loading was confirmed by parallel Coomassie-stained gels. For A and B, bar graphs show summary of densitometric analyses. For AQP2, bar graphs show the summation of bracketed and asterisked bands. Statistical significance was assessed by unpaired Student's t-test. *** P<0. 01 vs. *Atp6v1b1*$^{+/+}$. C. Immunohistochemistry on kidney sections showing AQP2 staining in renal medulla from *Atp6v1b1*$^{+/+}$ (upper panel) and *Atp6v1b1*$^{-/-}$ (lower panel) mice. Scale bars: 250 μm.

Figure 4: Effects of *Atp6v1b1* disruption on urine excretion of PGE_2 and ATP. Urinary excretion of PGE_2 (panel A) and ATP (panel B) in *Atp6v1b1*$^{-/-}$ and *Atp6v1b1*$^{+/+}$ mice. Data are the means ± S.E. For PGE_2, N= 26 to 27 mice in each group. For ATP, N= 15 mice in each group. Statistical significance was assessed by unpaired Student's t-test with Welch's correction. ** P<0.01 vs. *Atp6v1b1*$^{+/+}$; *** P<0.001 vs. *Atp6v1b1*$^{+/+}$.

Figure 5: Effects of 2 days of indomethacin injection on the protein abundance of ENaC, AQP2 and BKCa in *Atp6v1b1*$^{-/-}$ and *Atp6v1b1*$^{+/+}$ mice. Protein abundance of α-ENaC subunit (A and B), γ-ENaC subunit (C and D), AQP2 (E and F) and αBKCa (G and H) was assessed by Western blot of protein extracted from renal cortex (A, C, E and G) or medulla (B, D, F and H) of *Atp6v1b1*$^{-/-}$ (black bars) and *Atp6v1b1*$^{+/+}$ (white bars) mice after 2 days of indomethacin injections. Each lane was loaded with a protein sample from a different mouse.

15 µg and 5 µg proteins were loaded per gel lane for cortical samples and medullary samples, respectively. Equal loading was confirmed by parallel Coomassie-stained gels. Bar graphs show summary of densitometric analyses. *** $p<0.001$ vs. *Atp6v1b1*$^{+/+}$. In A and B, arrow indicates the 90 kDa specific band for α-ENaC. In E and F, bar graphs show the summation of bracketed (glycosylated 37 kDa form of AQP2) and asterisked (unglycosylated 25 kDa form of AQP2) bands.

Figure 6: Paracrine signaling in the isolated microperfused cortical collecting duct. A and B. Measurement of bafilomycin A1-induced luminal PGE_2 release in the isolated microperfused cortical collecting duct using a biosensor technique. A. HEK cells overexpressing the calcium-coupled PGE_2 receptor EP1 were loaded with the calcium-sensitive ratiometric fluorophore pair Fluo-4 and Fura Red, held by a holding pipette (HP1) and positioned in the lumen of the split-open microperfused connecting tubule-collecting duct in direct contact with the tubular fluid. PP: CCD perfusion pipette; HP2: a second holding pipette helped to keep the tubule-end in position. DIC image and fluorescence overlay are shown. B. Summary of PGE_2 biosensor responses. Fold change in Fluo-4/Fura Red fluorescence ratio is shown as index of PGE_2 release. Addition of 40 nM bafilomycin (Baf) to the bathing solution caused significant elevation in HEK-EP1 biosensor cell calcium indicating luminal PGE_2 release. The effects of bafilomycin were prevented by the addition of the purinergic (ATP) receptor blocker suramin (50 µM) to the tubular perfusate. Similarly, the selective PGE_2 EP1 receptor inhibitor SC51322 or SC (10 µM) added to the luminal perfusate blocked bafilomycin-induced biosensor responses indicating PGE_2 specificity. Addition of the ATP scavenger apyrase (50 U/ml) to the tubular perfusate also abolished PGE_2 biosensor responses consistent with its dependence on luminal ATP release. *: $P<0.05$ baf vs baseline (ctrl), n numbers per group are indicated in parentheses. C and D. Fluorescence imaging of bafilomycin-induced purinergic calcium signaling in the isolated microperfused cortical collecting duct. CCDs were perfusion-loaded with the calcium-sensitive ratiometric fluorophore pair Fluo-4 and Fura Red. C. Gradient pseudocolor images show CCD intracellular calcium ($[Ca^{2+}]_i$) levels before (left panel) and after (right panel) the addition of 40 nM bafilomycin to the bathing solution. Bafilomycin caused significant elevations in CCD $[Ca^{2+}]_i$, most significantly in ICs, which were identified based on anatomical considerations (lower cell density and higher cell volume compared to PCs). D. Summary of bafilomycin-induced changes in CCD $[Ca^{2+}]_i$. The purinergic (ATP) receptor blocker suramin added to the

tubular perfusate (50 μM) completely abolished the effects of bafilomycin. *: $P<0.05$ bafilomycin vs bafilomycin and suramin, n number per group is 5.

Figure 7: Schematic description of the consequence of vH-ATPase dysfunction on Na^+, K^+ and water transport in the CNT/CCD and the MCD. *Atp6v1b1* disruption impairs both electroneutral Na^+ absorption through β-ICs and ENaC-mediated Na^+ absorption through the neighboring principal cells (PC). Local ATP/PGE_2 signaling cascade is responsible for decreased ENaC protein and activity as well as AQP2 protein and contribute to Na^+ and water losses, thereby promoting high tubular flow. ENaC inhibition in the CNT/CCD likely blocks K^+ secretion through ROMK. In contrast, principal cells in the MCD have a normal response to hyperaldosteronism (i.e. increased ENaC expression). Increased ENaC activity in MCD is expected to favor K^+ secretion through ROMK. High tubular flow activates BKCa potassium channels and K^+ secretion, leading to renal K^+ loss in *Atp6v1b1*$^{-/-}$ mice. Indeed, indomethacin, which reduced urinary flow and restored AQP2 protein levels in *Atp6v1b1*$^{-/-}$ mice, also normalized protein levels of BKCa and decreased urinary K^+ excretion in *Atp6v1b1*$^{-/-}$ mice, leading to normal plasma potassium concentration.

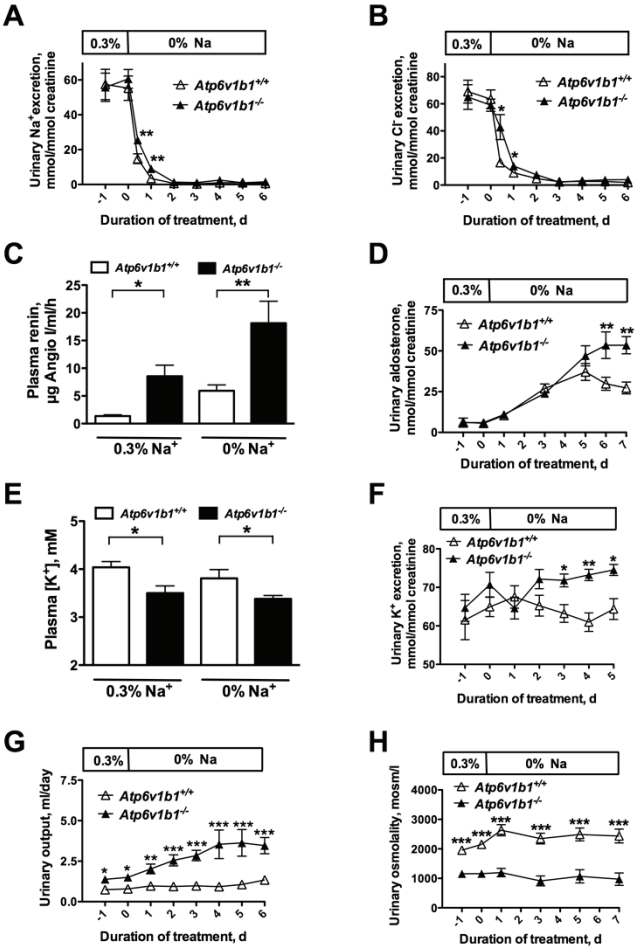
A
0.3%
0% Na
Urinary Na+excretion, mmol/mmol creatinine
Atp6v1b1+/+
Atp6v1b1-/-
Duration of treatment, d
B
Urinary Cl- excretion, mmol/mmol creatinine
C
Plasma renin, µg Angio I/ml/h
0.3% Na+
0% Na+
D
Urinary aldosterone, nmol/mmol creatinine
E
Plasma [K+], mM
F
Urinary K+ excretion, mmol/mmol creatinine
G
Urinary output, ml/day
H
Urinary osmolality, mosm/l

Figure 1

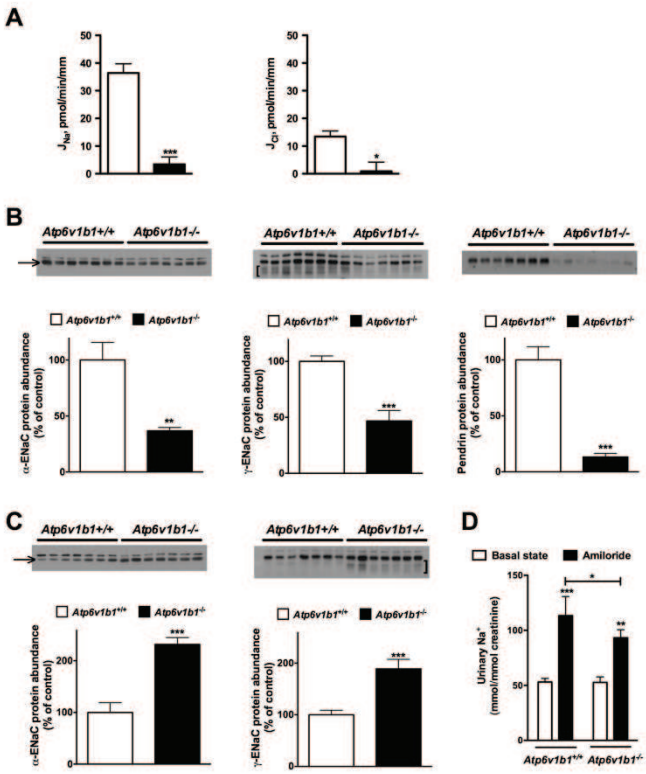
A
B
C
D
Atp6v1b1+/+
Atp6v1b1-/-
Basal state
Amiloride
α-ENaC protein abundance (% of control)
γ-ENaC protein abundance (% of control)
Pendrin protein abundance (% of control)
Urinary Na+ (mmol/mmol creatinine)

Figure 2

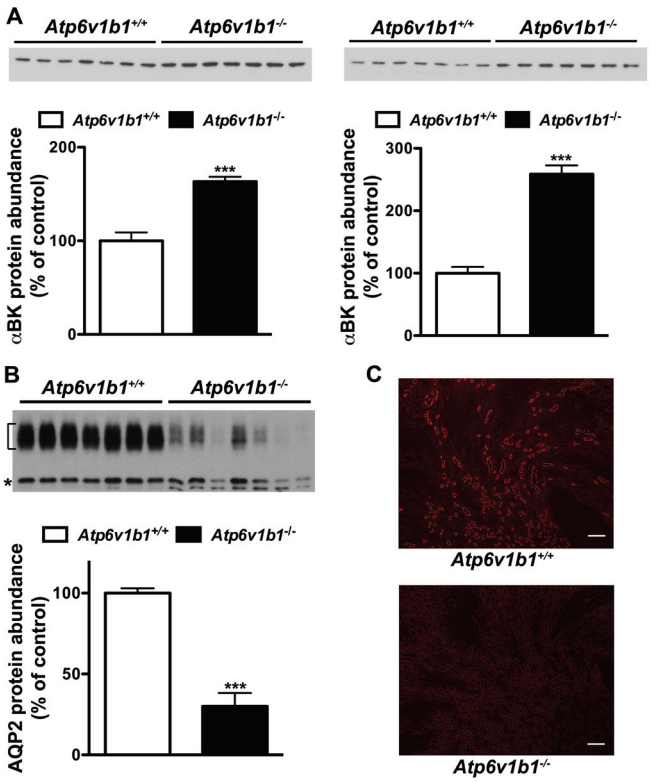
A
Atp6v1b1+/+
Atp6v1b1-/-
Atp6v1b1+/+
Atp6v1b1-/-
Atp6v1b1+/+
Atp6v1b1-/-
αBK protein abundance (% of control)
200
100
0
***
Atp6v1b1+/+
Atp6v1b1-/-
αBK protein abundance (% of control)
300
200
100
0
***
B
Atp6v1b1+/+
Atp6v1b1-/-
*
Atp6v1b1+/+
Atp6v1b1-/-
AQP2 protein abundance (% of control)
100
50
0
***
C
Atp6v1b1+/+
Atp6v1b1-/-

Figure 3

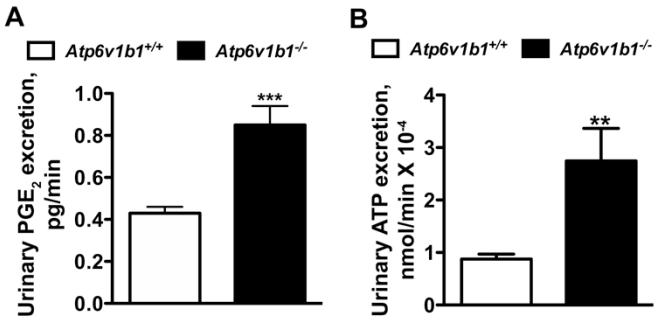
A
Atp6v1b1+/+
Atp6v1b1-/-
Urinary PGE2 excretion, pg/min
1.0
0.8
0.6
0.4
0.2
0.0
***
B
Atp6v1b1+/+
Atp6v1b1-/-
Urinary ATP excretion, nmol/min X 10-4
4
3
2
1
0
**

Figure 4

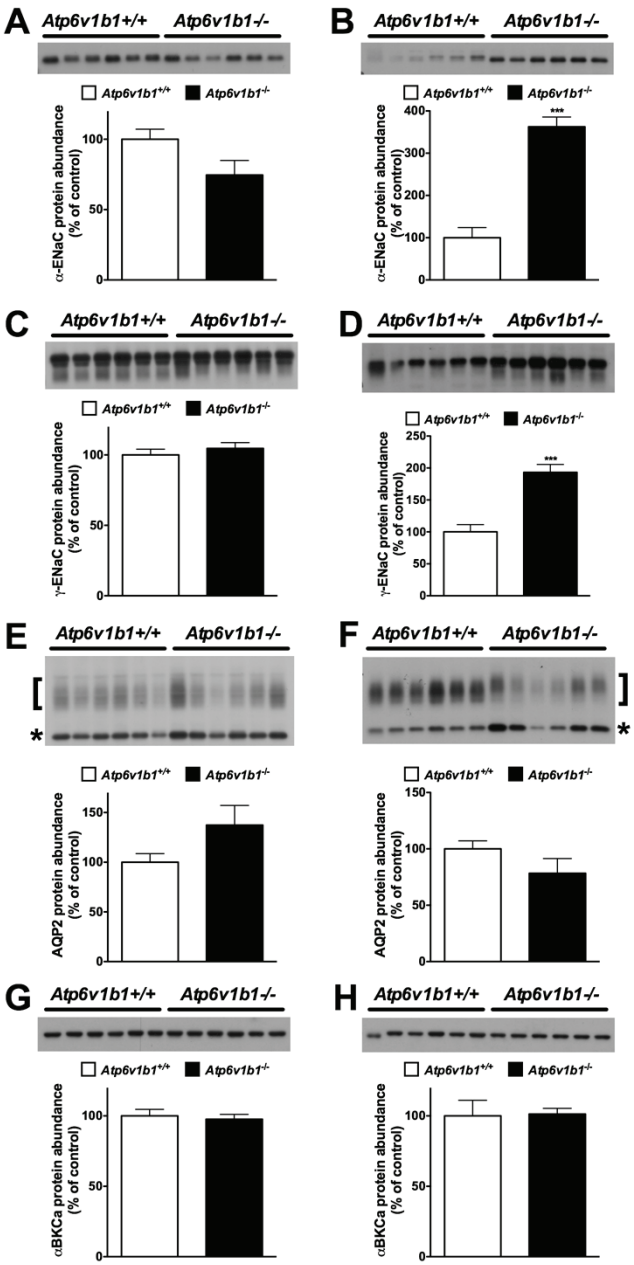
A
Atp6v1b1+/+
Atp6v1b1-/-
Atp6v1b1+/+
Atp6v1b1-/-
α-ENaC protein abundance (% of control)
100
50
0
B
Atp6v1b1+/+
Atp6v1b1-/-
Atp6v1b1+/+
Atp6v1b1-/-
α-ENaC protein abundance (% of control)
400
300
200
100
0
***
C
Atp6v1b1+/+
Atp6v1b1-/-
Atp6v1b1+/+
Atp6v1b1-/-
γ-ENaC protein abundance (% of control)
100
50
0
D
Atp6v1b1+/+
Atp6v1b1-/-
Atp6v1b1+/+
Atp6v1b1-/-
γ-ENaC protein abundance (% of control)
250
200
150
100
50
0
***
E
Atp6v1b1+/+
Atp6v1b1-/-
[
*
Atp6v1b1+/+
Atp6v1b1-/-
AQP2 protein abundance (% of control)
150
100
50
0
F
Atp6v1b1+/+
Atp6v1b1-/-
]
*
Atp6v1b1+/+
Atp6v1b1-/-
AQP2 protein abundance (% of control)
150
100
50
0
G
Atp6v1b1+/+
Atp6v1b1-/-
Atp6v1b1+/+
Atp6v1b1-/-
αBKCa protein abundance (% of control)
100
50
0
H
Atp6v1b1+/+
Atp6v1b1-/-
Atp6v1b1+/+
Atp6v1b1-/-
αBKCa protein abundance (% of control)
100
50
0

Figure 5

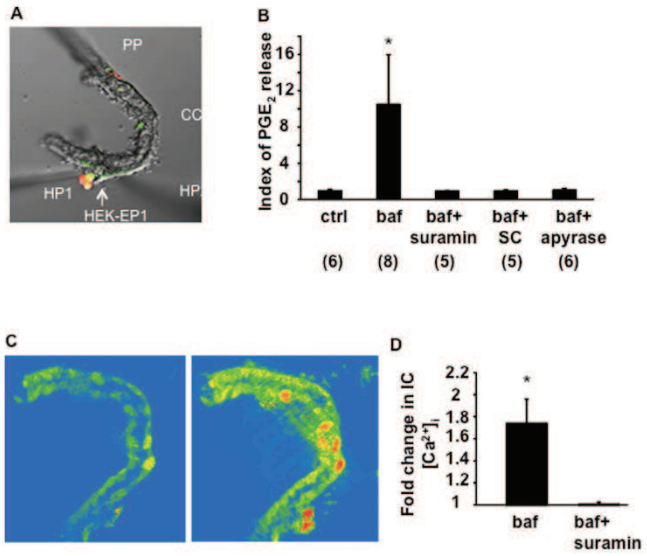
A
PP
CC
HP1
HP
HEK-EP1
B
Index of PGE2 release
16
12
8
4
0
*
ctrl
baf
baf+ suramin
baf+ SC
baf+ apyrase
(6)
(8)
(5)
(5)
(6)
C
D
Fold change in IC [Ca2+]i
2.2
2
1.8
1.6
1.4
1.2
1
*
baf
baf+ suramin

Figure 6

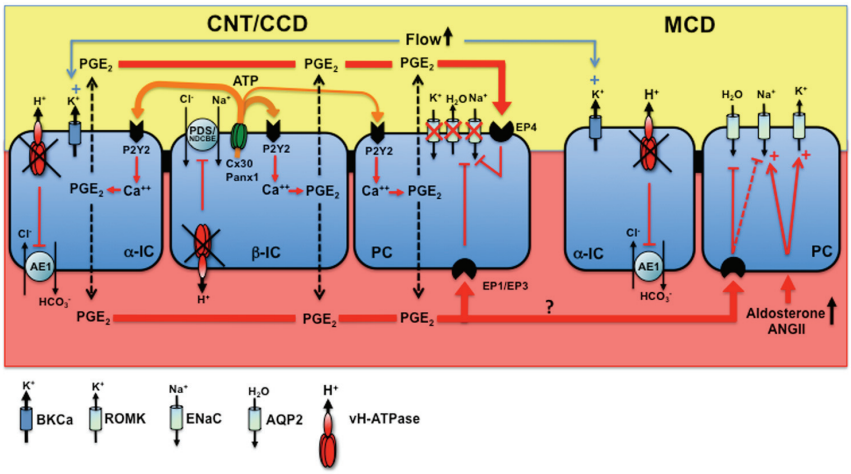
CNT/CCD
MCD
Flow
PGE2
ATP
H+
K+
Cl-
Na+
PDS/
NDCBE
Cx30
Panx1
P2Y2
Ca++
EP4
H2O
α-IC
β-IC
PC
AE1
HCO3-
EP1/EP3
?
Aldosterone
ANGII
BKCa
ROMK
ENaC
AQP2
vH-ATPase

Figure 7

Table 1: Summary of densitometric analyses of immunoblots on renal cortex and medulla homogenates from *Atp6v1b1*$^{+/+}$ and *Atp6v1b1*$^{-/-}$ mice without treatment and during indomethacin treatment (5 mg/kg/d for 48 hours) fed a normal diet (0.3% Na^+).

CORTEX	No treatment		48h indomethacin	
	Atp6v1b1$^{+/+}$ (n=7)	*Atp6v1b1*$^{-/-}$ (n=7)	*Atp6v1b1*$^{+/+}$ (n=6)	*Atp6v1b1*$^{-/-}$ (n=6)
αENaC	100 ± 9.0	48.0 ± 3.0***	100 ± 7.1	74.6 ± 10.4
γENaC (total)	100 ± 4.8	46.7 ± 9.3***	100 ± 4.1	104.6 ± 4.1
Pds	100 ± 11.8	13.3 ± 3.3***	100 ± 3.3	16.5 ± 4.4***
AQP2 (total)	100 ± 7	59 ± 13*	100 ± 8.6	137.3 ± 19.5
BK α subunit	100 ± 9	163.3 ± 5.2***	100 ± 4.6	97.6 ± 3.4
β-actin	100 ± 6.2	107.2 ± 4.6	100 ± 6.2	101.4 ± 4.0
MEDULLA	No treatment		48h indomethacin	
	Atp6v1b1$^{+/+}$ (n=7)	*Atp6v1b1*$^{-/-}$ (n=7)	*Atp6v1b1*$^{+/+}$ (n=6)	*Atp6v1b1*$^{-/-}$ (n=6)
αENaC	100 ± 18.9	231.6 ± 13.1***	100 ± 23.9	362.6 ± 23.1***
γENaC (total)	100 ± 8.8	188.8 ± 18.5***	100 ± 11.3	193.2 ± 12.4***
AQP2 (total)	100 ± 3.0	30.1 ± 8.3***	100 ± 7.1	78.4 ± 13.1
BK, α subunit	100 ± 10	258.8 ± 14***	100 ± 11.1	101.3 ± 4.0
ROMK	100 ± 21	176 ± 10**	100 ± 24	185 ± 5**
β-actin	100 ± 5.7	103.6 ± 5.5	100 ± 11.6	114 ± 4.3

Values are the means ± S.E. (n)= number of mice per group. Statistical significance between groups was determined by unpaired Student's t-test. * $p<0.05$; ** $p<0.01$; *** $p\leq0.001$ vs wild type mice.

Table 2: Physiological parameters from *Atp6v1b1*$^{-/-}$ mice before and during indomethacin treatment

	Basal state	24h indomethacin	48h indomethacin
Weight, g	24.4 ± 0.6	25.2 ± 0.6	25.0 ± 0.7
Food intake, g	4.18 ± 0.19	4.07 ± 0.24	3.79 ±0.23
Water intake, ml	7.69 ± 0.81	7.17 ±0.73	6.72 ± 0.39
Urine output, ml/24H	2.73 ± 0.2	1.97 ± 0.18**	1.98 ± 0.21*
Urine Osmolality, mosm/l	1564 ± 70	2048 ± 134**	1986 ± 122**
Urine Na, µmol /24H	248 ± 13	173 ± 31*	200 ± 33
Urine K, µmol/24H	697 ± 24	596 ± 50	574 ± 38*

Values are the means ± S.E. N= 12 mice. Statistical significance between groups was determined by unpaired Student's t-test. * $p<0.05$ vs basal state. ** $p\leq0.01$ vs basal state

SUPPLEMENTAL TABLES AND FIGURES

Table S1: Physiological blood parameters from *Atp6v1b1*$^{+/+}$ and *Atp6v1b1*$^{-/-}$ mice fed a normal diet (0.3% Na^+) or a low Na^+ diet (0% Na^+)

	0.3 % Na^+		**0 % Na^+**	
	Atp6v1b1$^{+/+}$	*Atp6v1b1*$^{-/-}$	*Atp6v1b1*$^{+/+}$	*Atp6v1b1*$^{-/-}$
pH	7.23 ± 0.01 (10)	7.26 ± 0.01 (9)	7.23 ± 0.01 (10)	7.27 ± 0.01 (9)*
PCO_2, mmHg	47.2 ± 1.8 (10)	50.0 ± 1.2 (9)	52.3 ± 1.8 (9)	52.2 ± 1.3 (9)
c[HCO_3^-], mmol/L	19.2 ± 0.9 (10)	21.5 ± 0.6 (9)*	21.2 ± 0.4 (10)	23.3 ± 0.8 (9)*
PO_2 mmHg	85.2 ± 1.8 (10)	93.9 ± 3.2 (9)*	83.3 ± 3.2 (10)	85.0 ± 3.6 (9)
[Na^+], mmol/L	147.8 ± 1.2 (9)	147.3 ± 0.7 (8)	147.1 ± 0.3 (10)	144.3 ± 0.8 (9)**
[K^+], mmol/L	4.04 ± 0.12 (10)	3.57 ± 0.15 (9)*	3.81 ± 0.18 (9)	3.38 ± 0.07 (9)*
[Cl^-], mmol/L	120.4 ± 0.9 (10)	121.0 ± 0.7 (9)	119.2 ± 0.4 (10)	115.1 ± 1.0 (9)**
[Proteins], g/L	45.7 ± 0.8 (10)	50.2 ± 1.2 (9)**	44.4 ± 1.3 (10)	53.1 ± 2.5 (8)**

Values are the means ± S.E (n), n= number of mice studied. Statistical significance between groups was assessed by unpaired Student's t-test. * $p<0.05$ vs wild type mice fed same diet; ** $p<0.01$ vs wild type mice fed same diet.

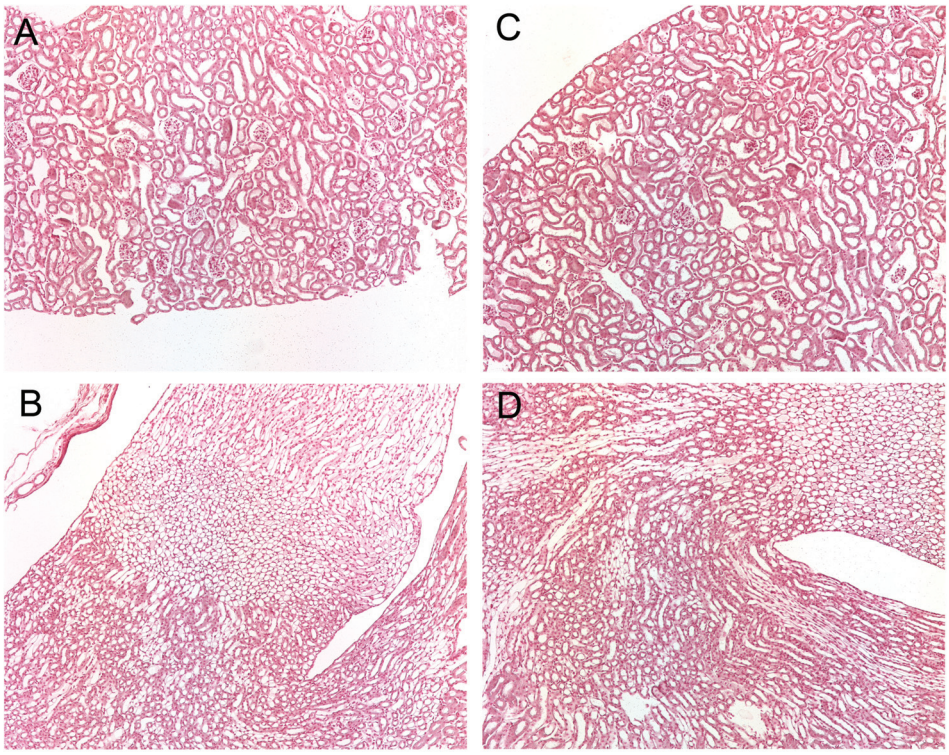

Figure S1

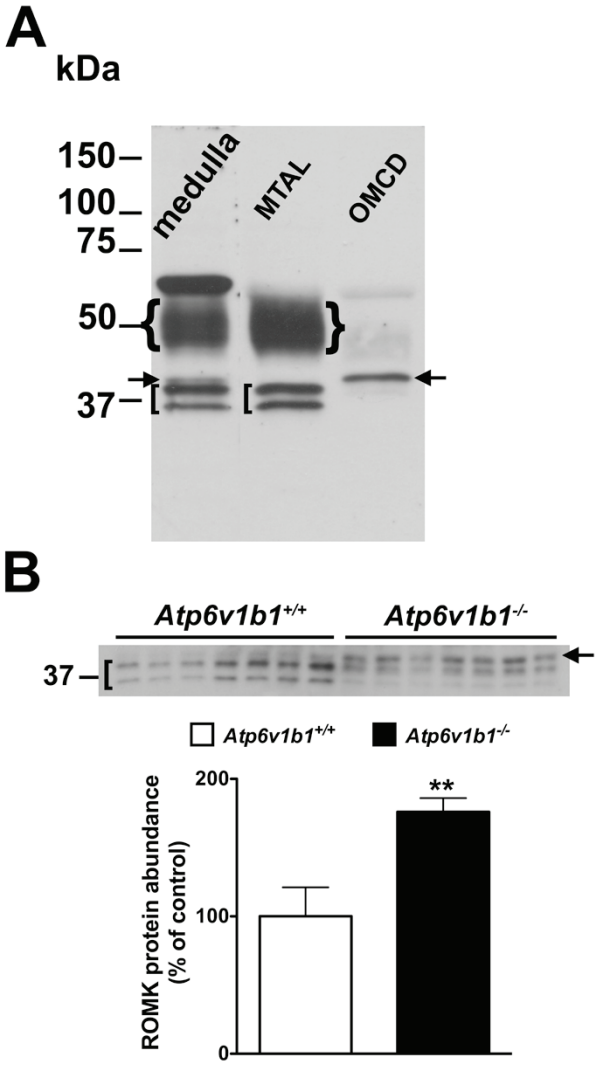
A
kDa
150
100
75
50
37
medulla
MTAL
OMCD
B
Atp6v1b1+/+
Atp6v1b1-/-
37
Atp6v1b1+/+
Atp6v1b1-/-
ROMK protein abundance
(% of control)
200
100
0
**

Figure S2

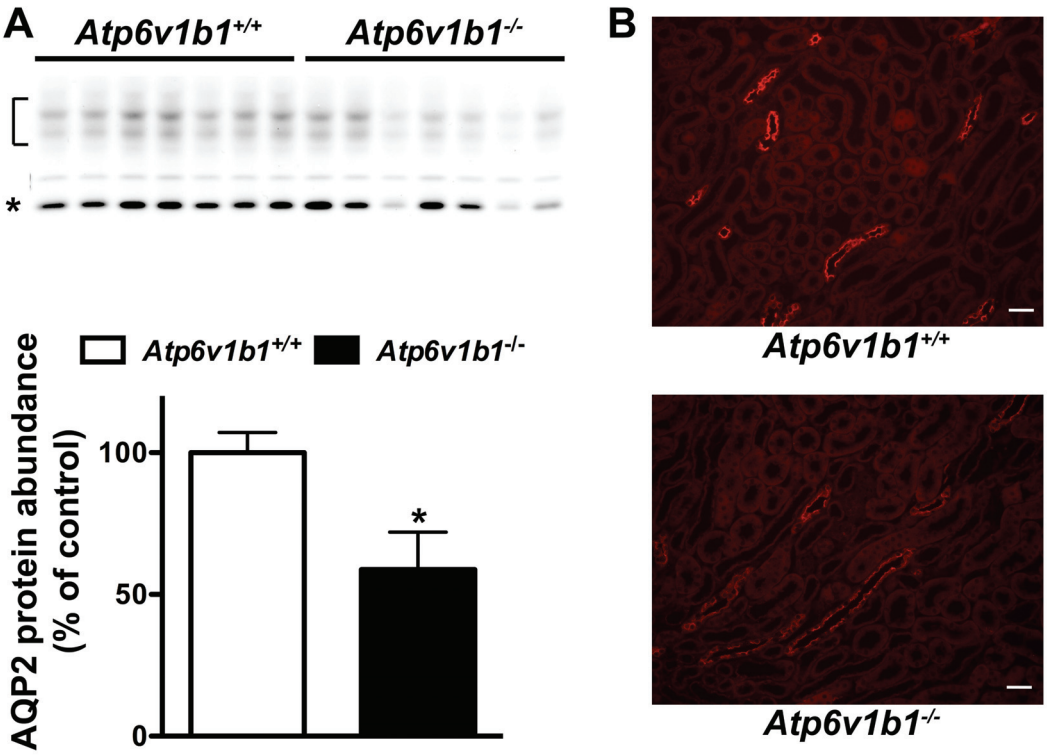
A
Atp6v1b1+/+
Atp6v1b1-/-
*
Atp6v1b1+/+
Atp6v1b1-/-
AQP2 protein abundance
(% of control)
100
50
0
*
B
Atp6v1b1+/+
Atp6v1b1-/-

Figure S3

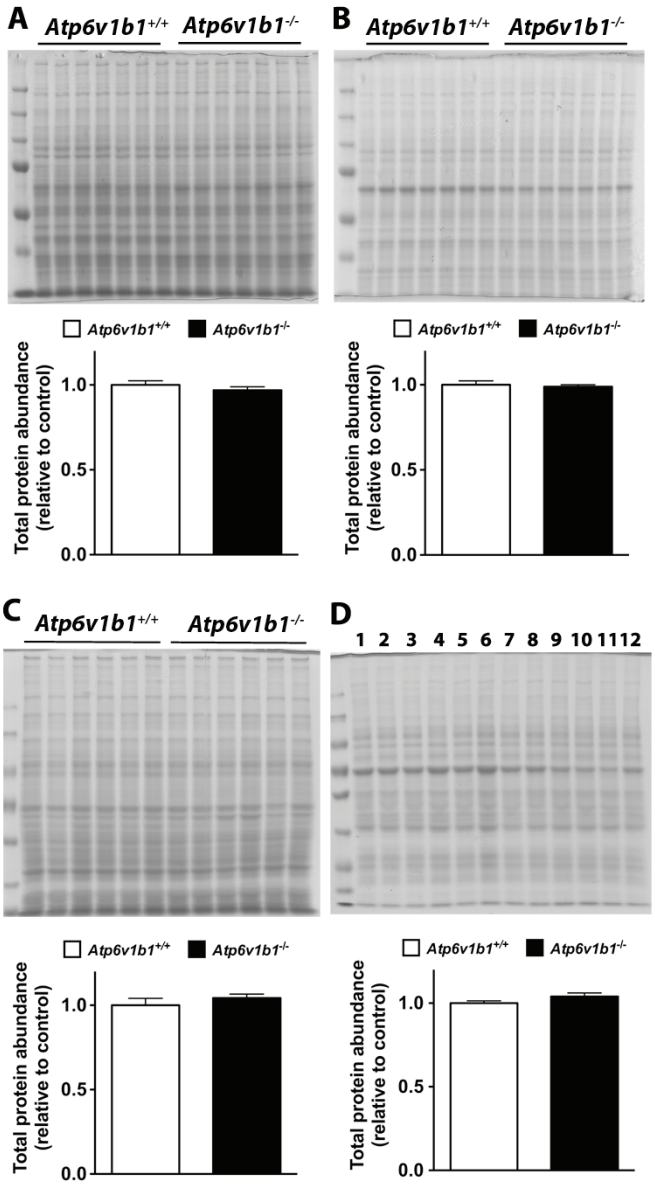
A
Atp6v1b1+/+
Atp6v1b1-/-
B
Atp6v1b1+/+
Atp6v1b1-/-
Atp6v1b1+/+
Atp6v1b1-/-
Total protein abundance (relative to control)
1.0
0.5
0.0
Atp6v1b1+/+
Atp6v1b1-/-
Total protein abundance (relative to control)
1.0
0.5
0.0
C
Atp6v1b1+/+
Atp6v1b1-/-
D
1 2 3 4 5 6 7 8 9 10 11 12
Atp6v1b1+/+
Atp6v1b1-/-
Total protein abundance (relative to control)
1.0
0.5
0.0
Atp6v1b1+/+
Atp6v1b1-/-
Total protein abundance (relative to control)
1.0
0.5
0.0

Figure S4

LEGENDS FOR SUPPL. FIGURES

Figure S1: Von Kossa stainings of sections of kidneys from *Atp6v1b1*$^{-/-}$ and *Atp6v1b1*$^{+/+}$
A, renal cortex from *Atp6v1b1*$^{+/+}$ mouse, B renal medulla from *Atp6v1b1*$^{+/+}$ mouse, C renal cortex from *Atp6v1b1*$^{-/-}$ mouse, and D renal medulla from *Atp6v1b1*$^{-/-}$ mouse.

Figure S2: Western blots for ROMK on kidney samples. A. Molecular profiling of ROMK was assessed by Western blots in renal medullary homogenate (medulla), medullary thick ascending limbs (MTAL) or outer medullary collecting ducts (OMCD) from *Atp6v1b1*$^{+/+}$ mice. In MTAL, anti ROMK antibody detects a broad band centered at 50kDa (curly bracket) and a doublet at 37 kDa (square bracket). In OMCD, anti ROMK antibody detects a major band that migrated above 37 kDa (arrow). A broad 50 kDa band was barely detected. In medulla, anti ROMK antibody detects bands that were seen in MTAL (the broad band centered at 50 kDa –curly bracket- and the doublet centered at 37 kDa – square bracket-) plus the band above 37kDa (arrow) that was seen in OMCD. Anti ROMK antibody also detects an additional sharp 65 kDa band (asterisk). 5 µg proteins of medullary homogenate or approximatively 40 tubule segments were loaded per gel lane. **B.** Effects of *Atp6v1b1* disruption on ROMK protein expression in medullary collecting ducts. ROMK protein abundance was assessed by Western blots of medullary homogenates from *Atp6v1b1*$^{-/-}$ and *Atp6v1b1*$^{+/+}$. Each lane was loaded with a protein sample from a different mouse. 5 µg proteins were loaded per gel lane. Equal loading was confirmed by parallel Coomassie-stained gels. Anti ROMK antibody detects a triplet around 37 kDa in which the upper band corresponds to the molecular form of ROMK expressed exclusively in the collecting duct (arrow), whereas the two lower bands are polypeptides whose expression is restricted to the thick ascending limb (square bracket). Bar graph shows summary of densitometric analyses of the upper band (arrow). Statistical significance was assessed by unpaired Student's t-test. ** $P<0.01$ vs. *Atp6v1b1*$^{+/+}$

Figure S3: AQP2 expression assessed in *Atp6v1b1*$^{-/-}$ and *Atp6v1b1*$^{+/+}$ mice by Western blot on renal cortex (A) or immunohistochemistry on kidney sections (B). A. Each lane was loaded with a protein sample from a different mouse. Equal loading was confirmed by parallel Coomassie-stained gels. 15 µg proteins were loaded per gel lane. Bracket and asterisk show the glycosylated 37 kDa and the unglycosylated 25 kDa forms of AQP2, respectively.

Bar graph shows summary of densitometric analyses of the bracketed and asterisked bands. Statistical significance was assessed by unpaired Student's t-test. * $P<0.05$ vs. *Atp6v1b1*$^{+/+}$. B. Renal cortex from *Atp6v1b1*$^{+/+}$ (upper panel) and *Atp6v1b1*$^{-/-}$ (lower panel) mice. Scale bars: 100 μm.

Figure S4: Representative Coomassie blue-stained polyacrylamide gels used to control protein loading. Protein samples loaded on gels are the same as those used for subsequent Western blots. A. Whole cortex homogenates from *Atp6v1b1*$^{+/+}$ or *Atp6v1b1*$^{-/-}$ mice. B. Whole medulla homogenates from *Atp6v1b1*$^{+/+}$ or *Atp6v1b1*$^{-/-}$ mice. C. Whole cortex homogenates from indomethacin treated *Atp6v1b1*$^{+/+}$ or *Atp6v1b1*$^{-/-}$ mice. D. Whole medulla homogenates from indomethacin treated *Atp6v1b1*$^{+/+}$ (odd numbers) or *Atp6v1b1*$^{-/-}$ (even numbers) mice. 15 μg proteins per lane were loaded on gels A and C. 5 μg proteins per lane were loaded on gels B and D. Bands from these gels were analyzed using densitometry to provide quantitative assessment of loading. Density values were normalized by dividing values by the mean value for the entire set of samples. Thus the mean for the entire set of samples is defined as 1. Normalized density values were never below 0.85 or higher than 1.15. To facilate comparisons between groups, density values were normalized by dividing by the mean value for the control group. Thus the mean for the control group is defined as 1. Bar graphs show summary of these densitometric analyses. Normalized band densities for mutants were compared with controls using an unpaired *t*-test. Values are means ± S.E.. In all gels, no difference was noted between control and mutant mice. These loading gels established that subsequent immunoblots (loaded identically) were uniformly loaded.